ACSAF validation report on the EUMETSAT IASI/Metop CDR SO_2 datasets

Validated products:

Name	Satellites
SO_2 total column SO_2 altitude O3M-540	Metop-A, Metop-B

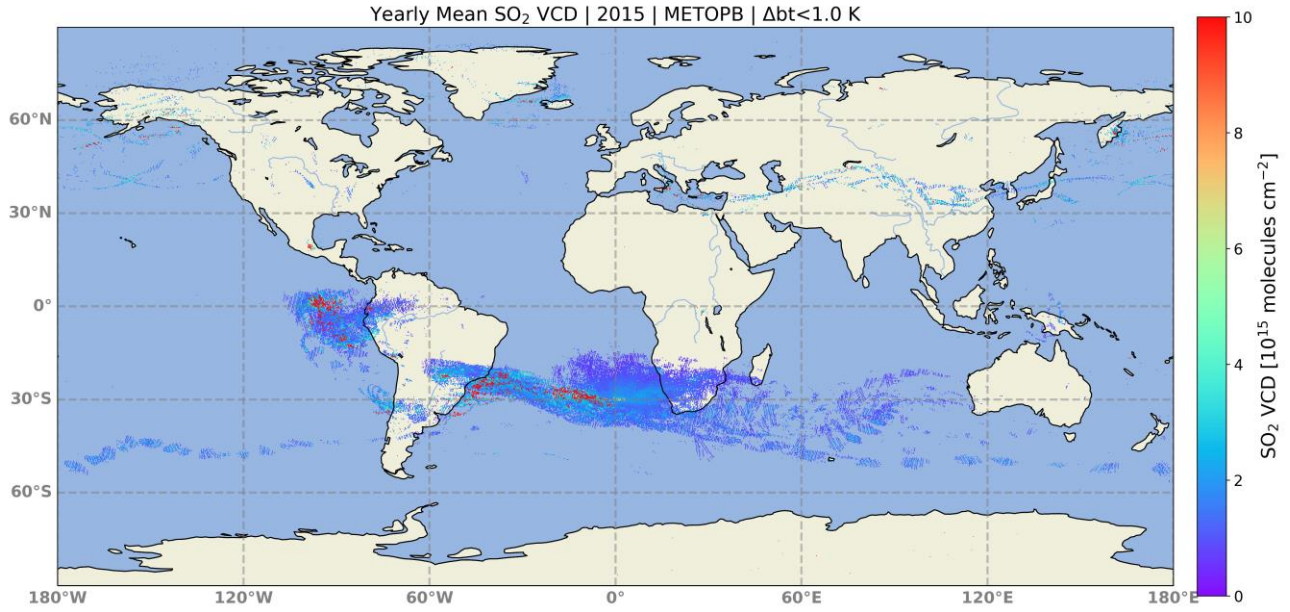

Yearly mean SO_2 vertical column density for 2015 including the Calbuco, Chile, eruption and a Mt Etna, Italy, eruption which transported SO_2 over Asia.

Authors: Name	Institute
MariLiza Koukouli	Laboratory of Atmospheric Physics
Gaia Pinardi	Belgian Institute for Space Aeronomy

Reporting period:	IASI/MetopA | Oct 2007 – Oct 2021 IASI/MetopB | Feb 2013 - Dec 2021
Input data versions:	IASI/MetopA & /MetopB EUMETSAT netcdf
Data processor versions:	Brescia v6.6

Introduction to EUMETSAT Satellite Application Facility on Atmospheric Composition monitoring (AC SAF)

Background

The monitoring of atmospheric chemistry is essential due to several human caused changes in the atmosphere, like global warming, loss of stratospheric ozone, increasing UV radiation, and pollution. Furthermore, the monitoring is used to react to the threats caused by natural hazards as well as follow the effects of the international protocols.

Therefore, monitoring the chemical composition and radiation of the atmosphere is a very important duty for EUMETSAT and the target is to provide information for policy makers, scientists and the general public.

Objectives

The main objectives of the AC SAF is to process, archive, validate and disseminate atmospheric composition products (O_3, NO_2, SO_2, BrO, HCHO, H_2O, OClO, CO, NH3), aerosol products and surface ultraviolet radiation products utilising the satellites of EUMETSAT. The majority of the AC SAF products are based on data from the GOME-2 and IASI instruments onboard Metop satellites.

Another important task besides the near real-time (NRT) and offline data dissemination is the provision of long-term, high-quality atmospheric composition products resulting from reprocessing activities.

Product categories, timeliness and dissemination

NRT products are available in less than three hours after measurement. These products are disseminated via EUMETCast, WMO GTS or internet.

- Near real-time trace gas columns (total and tropospheric O_3 and NO_2, total SO_2, total HCHO, CO) and high-resolution ozone profiles
- Near real-time absorbing aerosol height and absorbing aerosol index from polarization measurement detectors
- Near real-time UV indexes, clear-sky and cloud-corrected

Offline products are available within two weeks after measurement and disseminated via dedicated AC SAF web services.

- Offline trace gas columns (total and tropospheric O_3 and NO_2, total SO_2, total BrO, total HCHO, total H_2O) and high-resolution ozone profiles
- Offline absorbing aerosol height and absorbing aerosol index from polarization measurement detectors
- Offline surface UV, daily doses and daily maximum values with several weighting functions

Data records are available after reprocessing activities from the AC SAF archives.

- Data records generated in reprocessing
- Lambertian-equivalent reflectivity
- Total OClO

Users can access the AC SAF offline products and data records (free of charge) by registering at the AC SAF web site.

More information about the AC SAF project, products and services: https://acsaf.org/

AC SAF Helpdesk: helpdesk@acsaf.org

Twitter: https://twitter.com/Atmospheric_SAF

Applicable documents

[ATBD] ALGORITHM THEORETICAL BASIS DOCUMENT, IASI Brescia SO2 columns and SO_2 altitude, Clarisse, L., Daniel Hurtmans, Pierre-François Coheur, Rosa Astoreca, Maya George and Cathy Clerbaux, SAF/AC/ULB/BresciaSO2_ATBD, issue: 1.3, date: 01/02/2021.

[PRD] Product Requirements Document SAF/AC/FMI/RQ/PRD/001 Issue 2.0, 02/12/2022, https://acsaf.org/team/doc/prd/saf_ac_prd_i2r0_20221202.pdf, last accessed: 17.03.2023.

[PUM] Product User manual, IASI Reprocessed SO_2 CDR (O3M-540), R. Astoreca, D. Hurtmans, L. Clarisse, P. Coheur, J. Hadji-Lazaro, M. George, C. Viatte, C. Clerbaux, M. Doutriaux-Boucher, C. Vicente and M. Crapeau, SAF/AC/ULB/PUM/010, 1.1, 28/02/2023.

[VR] IASI-C ACSAF VALIDATION REPORT, Koukouli, M. E., Pinardi, G. and Langerock, B., SAF/AC/AUTH/VR/IASI_SO2 01/2021, issue: 01/2021, date: 30/4/2021, https://acsaf.org/docs/vr/Validation_Report_IASI-C_SO2_Apr_2021.pdf, last accessed: 03.04.2023

Authors

Gaia Pinardi, BIRA, authored section 3.2, while MariLiza Koukouli, AUTH, is responsible for the rest of the document. The summary and recommendations section is approved by both authors.

Acknowledgments

Part of the results presented in this work have been produced using the Aristotle University of Thessaloniki High Performance Computing Infrastructure and Resources. M.E.K. would like to acknowledge the support provided by the IT Center of the Aristotle University of Thessaloniki throughout the progress of this research work. We further warmly acknowledge the support by the Atmospheric Toolbox®.

Gaia Pinardi wishes to thank Bavo Langerock and Michel Van Roozendael who respectively helped in checking and pre-processing IASI data and in analysing some of the ground-based SO_2 datasets.

TABLE OF CONTENTS

1. INTRODUCTION 7

2. IASI/METOP SULPHUR DIOXIDE COLUMN AND PLUME HEIGHT 8

2.1 The IASI/Metop CDR SO_2 products 8
2.1.1 SO_2 vertical column density and SO_2 altitude 8
2.1.2 Volcanic SO_2 sources 8
2.2 Inter-sensor investigations 9
2.2.1 Investigation on the ΔBt flag 9
2.2.2 Inter-sensor consistency 10

3. SULPHUR DIOXIDE COLUMN VALIDATION 13

3.1 Validation against S5P/TROPOMI 13
3.2 Comparisons against the MAX-DOAS network 15
3.2.1 Conclusions from the comparisons with the BIRA-IASB ground-based stations 33

4. SULPHUR DIOXIDE ALTITUDE VALIDATION 36

4.1.1 S5P/TROPOMI SO_2 Layer Height 36
4.1.2 Volcanic eruptions studied 37
4.1.3 Comparisons with the S5P/TROPOMI SO_2 layer height 38

5. SUMMARY AND RECOMMENDATIONS 42

REFERENCES 43

APPENDIX 45

Table of Figures

Figure 1. The effect of the ΔBt recommended cut-off on the IASI SO_2 reported loads for three major eruptions during the IASI-A timeline. Left column, ΔBt > 0.4K and right column, ΔBt > 1K. 10
Figure 2. The IASI-A [left] and IASI-B [right] ΔBt > 1K SO_2 loads during the Ambae, 2018 eruption [upper] and the Kelut, 2014 eruption [lower]. 11
Figure 3. Histograms of the IASI-A [blue] and IASI-B [orange] ΔBt > 1K SO_2 loads during six concurrent volcanic eruptions between 2014 and 2020 in temporal sequence. Names and time periods are insert in the titles. 12
Figure 4. S5P daily volcanic SO_2 VCD at 7km for three major eruptions, Sierra Negra and Ambae, in 2018, and Raikoke, in 2019 shown on the left column and the IASI-A ΔBt> 1K observations for the same eruptions on the right column. 14
Figure 5. Same-pixel comparison of SO_2 mass [kt/day] for the Ambae [upper] and the Raikoke [lower] eruptions between S5P and IASI-A [left] and IASI-B [right]. 15
Figure 6.IASI-A SO_2 columns overpasses around the BIRA-IASB stations; SO_2 VCD estimates for 13km (blue dots), 16km (red dots) and for the retrieved height (green dots). Two filtering cases are shown, for ΔBt > 0.4K (top) and ΔBt > 1K (bottom). 17
Figure 7. IASI-B SO_2 columns overpasses around the BIRA-IASB stations for ΔBt > 1K; SO_2 VCD estimates for 13km (blue dots), 16km (red dots) and for the retrieved height (green dots). 18
Figure 8. Uccle SO_2 VCD time-series of the IASI-A and IASI-B overpasses (colored squares) and the analyzed ground-based data (black dots). Top: the whole time-series; Lower Left: June 2011 Grimsvotn eruption; Right: July 2019 Raikoke eruption. 21

Figure 9. SO_2 VCD comparisons at Uccle for 2 days focusing on the Grimsvotn eruption in 2011, left and right columns. Each figure contains an upper panel with the SO_2 VCD time-series from the zenith measurements (in red) and from IASI (columns at the retrieved height, color-coded as a function of the station distance). The lower panel presents the geographical distribution of the IASI SO_2 VCD around the station (circles at 50km and 100km are plotted in dotted lines). 21
Figure 10. SO_2 VCD comparisons at Uccle focusing on the July 2019 eruption (Raikoke). Days are left to right, top to bottom. Each panel present an upper panel, with the SO_2 VCD time-series from the zenith measurements (in red) and from IASI (columns at the retrieved height, color-coded as a function of the station distance; circles for IASI-A, squares for IASI-B). The second panel presents the geographical distribution of the IASI-A (left) and IASI-B (right) SO_2 VCD around the station (circles at 50km and 100km are plotted in dotted lines). 22
Figure 11. Jungfraujoch SO_2 VCD time-series of the IASI-A (left) and IASI-B (right) overpasses (colored squares) and the analyzed ground-based data (black dots). Up: the whole 2007-2021 time-series; Bottom left: zoom on June 2011 for the Grimsvotn eruption; Bottom right: zoom on summer 2019 for the Raikoke eruption. 23
Figure 12. SO_2 VCD comparisons at Jungfraujoch on 6/6/2011 for the Grimsvotn eruption. The figure presents an upper panel, with the SO_2 VCD time-series from the zenith measurements (in red) and from IASI-A (SO_2 columns at the retrieved height, color-coded as a function of the station distance). The lower panels present the geographical distribution of the IASI-A SO_2 VCD around the station (circles at 50km and 100km are plotted in dotted lines). 24
Figure 13. SO_2 VCD comparisons at Jungfraujoch on 23/11/2013 for an Etna eruption. The figure presents an upper panel, with the SO_2 VCD time-series from the zenith measurements (in red) and from IASI-A (circles) and IASI-B (squares) (SO_2 columns at the retrieved height, color-coded as a function of the station distance, for all pixels with $\Delta Bt>0.4K$ within 80km of the station). The lower panels present the geographical distribution of the IASI-A SO_2 VCD around the station (circles at 50km and 100km are plotted in dotted lines).....25
Figure 14. Bujumbura SO_2 VCD time-series of the IASI overpasses (colored squares). Left: the whole 2007-2021 time-series; right: zoom on Nyamuragira eruption of 6/11 to 6/12/2011. 25
Figure 15. Bujumbura SO_2 VCD time-series of the 2013-2016 IASI-A (left) and IASI-B (right) overpasses (colored squares and the available retrieved ground-based data (black dots). 25
Figure 16. SO_2 VCD comparisons at Bujumbura for different eruptive days. The figure presents an upper panel, with the SO_2 VCD time-series from the zenith measurements (in red) and from IASI-A (circles) and IASI-B (squares) (SO_2 columns at the retrieved height, color-coded as a function of the station distance). The lower panels present the geographical distribution of the IASI-A (left) and IASI-B (right) SO_2 VCD around the station (circles at 50km and 100km are plotted in dotted lines). 27
Figure 17. Reunion SO_2 VCD time-series of the IASI overpasses (colored squares) and the analyzed ground-based data (black dots). Left: the whole 2007-2021 time-series; Right: zoom on July 2019 for the Ubinas plume on the 23th. 27
Figure 18. SO_2 VCD comparisons at Reunion focusing on the Ubinas eruption on 23/07/2019. The figure presents an upper panel, with the SO_2 VCD time-series from the zenith measurements (in red) and from IASI-A (circles) and IASI-B (squares) (SO_2 columns at the retrieved height, color-coded as a function of the station distance). The lower panels present the geographical distribution of the IASI-A (left) and IASI-B (right) SO_2 VCD around the station (circles at 50km and 100km are plotted in dotted lines).....28
Figure 19. Xianghe SO_2 VCD time-series of the IASI-A and IASI-B overpasses (colored squares) and the analyzed ground-based data (black dots). Top row: the whole time-series; bottom: June 2011 Nabro eruption (left) and December 2020 (right). 29
Figure 20. SO_2 VCD comparisons at Xianghe for total SO_2 from direct sun geometry (in green) and tropospheric SO_2 VCD from MAXDOAS (in blue). 30

Figure 21. SO_2 VCD comparisons at Xianghe focusing on June 2011. The first panel shows total SO_2 from direct sun geometry (in green) and tropospheric SO_2 VCD from MAXDOAS (in blue). The second panel shows stratospheric SO_2, as retrieved from the total minus tropospheric VCD (in black) and as retrieved using a stratospheric AMF from zenith measurements (in red). 30
Figure 22. SO_2 VCD comparisons at Xianghe focusing on June 2011 around the Nabro plume overpass. IASI columns in a radius of 300km around the stations are reported for different heights and the stratospheric VCD are estimated from the total direct sun minus tropospheric MAXDOAS VCD (in black) and from zenith measurements with a fixed DOAS reference taken on 12/06/2011 at noon (in red). 31
Figure 23. SO_2 VCD comparisons at Xianghe focusing on the 18 to 22 June 2011. Days are left to right, top to bottom. Each day present an upper panel, with the SO_2 VCD time-series reported from the total direct sun minus tropospheric MAXDOAS (in black), from the zenith measurements (in red) and from IASI-A (columns at the retrieved height, color-coded as a function of the station distance). The second panel presents the geographical distribution of the IASI SO_2 VCD around the Xianghe station (circles at 50km and 100km are plotted in dotted lines) for the day (left) and the night (right) overpasses. 32
Figure 24. SO_2 VCD comparisons at Xianghe focusing on the 25 December 2020. In the upper panel, the SO_2 VCD time-series are reported from the zenith measurements (in red) and from IASI-A (dots) and IASI-B (squares) (SO_2 columns at the retrieved height, color-coded as a function of the station distance). The lower panels present the geographical distribution of the IASI-A (left) and IASI-B (right) SO_2 VCD around the Xianghe station (circles at 50km and 100km are plotted in dotted lines) for the day (left) and the night (right) overpasses. 33
Figure 25. Illustration of the quantitative comparison method for Uccle on 13/07/2019, taking 30-minutes averages (squares) from the original ground-based and IASI datasets. 33
Figure 26. SO_2 VCD comparisons summary for the different IASI SO_2 estimates: SO_2 retrieved height (upper) and fixed 10km height (lower) for IASI-A (left) and IASI-B (right). 35
Figure 27. Examples of the IASI-A [left] and IASI-B [right] $\Delta Bt > 1K$ SO_2 plume height during the Taal 2020 eruption [upper] and the Raikoke 2019 eruption [lower]. Note that during Raikoke, there was a synchronous volcanic eruption in Indonesia. 38
Figure 28. The second day of the Raikoke eruption, on the 24th of June 2019, is shown for the S5P SO_2 layer height [upper], the IASI-A SO_2 plume height [middle] and the IASI-B SO_2 plume height [lower] for IASI data with $\Delta Bt > 0.4$ K [left column] and $\Delta Bt > 1K$ [right column.] 39
Figure 29. The fifth day of the Raikoke eruption, on the 27th of June 2019, is shown for the S5P SO_2 layer height [upper], the IASI-A SO_2 plume height [middle] and the IASI-B SO_2 plume height [lower] for IASI data with $\Delta Bt > 0.4$ K [left column] and $\Delta Bt > 1K$ [right column.] 40
Figure 30. Scatter plot of the daily mean SO_2 heights sensed by S5P, IASI-A [blue] and IASI-B [green] for all eruptive periods enumerated in Table 6. Upper plot for IASI data with $\Delta Bt > 0.4$ K and lower plot for IASI data with $\Delta Bt > 1.0$ K. 41

Table of Tables

Table 1. Selected volcanic emissions studied within this work. 9
Table 2. Comparison of the mean SO_2 load per eruption between S5P, IASI-A and IASI-B. 14
Table 3. Information on BIRA-IASB sites, with relevant details for SO_2 retrievals possibilities. 19
Table 4. Mean SO_2 VCD values for the ground-based and IASI-A different options, for the good condition cases (pixels from daily overpass within 80km of the station). 34
Table 5. Mean SO_2 VCD values for the ground-based and IASI-B different options, for the good condition cases (pixels from daily overpass within 80km of the station). 34
Table 6. Daily mean SO_2 height [km] for all eruptive days shown in Figure 30, bottom panel. 45

1. INTRODUCTION

The main aim of this validation report is to testify as to the capability of the EUMETSAT operational algorithm v6.6 to accurately retrieve IASI/MetopA and /MetopB total SO_2 columns and SO_2 plume heights on a global scale.

The validation exercise is performed on orbital netcdf files created by EUMETSAT for the needs of the ACSAF team, communicated via a sftp location. Inherent in the netcdf file metadata is the following pertinent information:

summary = "This file contains the Release 1 IASI L2 reprocessed for one orbit. The reprocessing was done on Linux using an adapted version of the EUMETSAT operational algorithm V6.6. Until December 2016, the reprocessed Metop-A IASI L1C input data were used (doi:10.15770/EUM_SEC_CLM_0014), after this date and for Metop-B the operational IASI L1c were used; this is to produce an homogeneous CDR. ERA5 were used as auxiliary model data"

processing_centre = "CDR"

processing_mode = "R"

project = "This data is provided as part of the EUMETSAT Satellite Application Facility on Atmospheric Composition Monitoring service, AC-SAF"

id = "DOI: 10.15770/EUM_SAF_AC_0046"

history = "Release 1"

title = "IASI SO2 CDR Release 1"

title_short_name = "IASI SO2 CDR"

keywords = "IASI SO2 CDR Climate"

The time span of the delivered datasets is:

IASI/MetopA | 01 Jan 2008 to 15 Oct 2021

IASI/MetopB | 20 Feb 2013 to 31 Dec 2021

2. IASI/METOP SULPHUR DIOXIDE COLUMN AND PLUME HEIGHT

2.1 The IASI/Metop CDR SO_2 products

The Brescia retrieval scheme includes two algorithms. The first algorithm, for the sounding of SO_2 above ~5 km altitude, includes as main features a wide applicable total column range (over 4 orders of magnitude, from 0.5 to 5000 D.U.), a low theoretical uncertainty (3-5 %) and near real time applicability. The output consists of 5 different hypothetical SO_2 columns, for this version at 7, 10, 13, 16 and 25 km, depending on the altitude of the SO_2 plume in question, and is meant to be used with auxiliary altitude data. A typical use-case is where a user will have an estimate of the SO_2 altitude (provided by e.g. a model or third party measurements), and in that case, the user can interpolate the 5 SO_2 columns to this estimate to obtain a single SO_2 column.

These different SO_2 columns which depend on different SO_2 plume heights have already been validated using previous versions of the IASI datasets, in the official validation reports for IASI-A and IASI-B and for IASI-C. In the current validation report, we will focus on the retrieval by the second algorithm where information on the SO_2 altitude can also be retrieved directly from the IASI measurement. As a result, an interpolated SO_2 column (from the first algorithm), at the retrieved SO_2 altitude (from the second algorithm) is also provided. This SO_2 column product, and the associated retrieved SO_2 altitude are validated in this report.

Refer to the [PUM] and the [ATBD] for further information on the IASI Brescia products.

2.1.1 SO_2 vertical column density and SO_2 altitude

In this work, the *so2_col* variable included in the netcdf files provided by EUMETSAT is being assessed, which represents the *SO_2 column at the retrieved plume altitude from a neural network approach*, as well as the *so2_altitudes* variable which represents the *retrieved plume altitude*. Two further variables are also utilized, namely the *so2_qflag*, general quality flags and the *so2_bt_difference*, which represents an i*ndicative brightness temperature difference*; it is recommended to only keep the data for which this difference is greater than 0.4.

With respect to the *so2_qflag*, it is stated in the [PUM] that all retrieved SO_2 columns are considered best quality retrievals and can be used. However, when the *so2_qflag* is set to either 0 or 9 this identifies retrievals which used the IASI L2 pressure and temperature profiles. When the *so2_qflag* is set to either 1 or 11, this means that the pressure and temperature profiles are missing in the IASI L2 data and that model/forecast data have been used instead. In the following, pixels retrieved with the IASI L2 temperature and pressure profiles were allowed for the analysis.

With respect to the *so2_bt_difference*, it is stated in the [PUM] only look at the retrievals in the neighbourhood of $\Delta Bt>1K$ pixels, and not use at all any pixels with an associated $\Delta Bt <0.4K$, which means that there is not enough SO_2 to have a reliable retrieval. It is further stated that size of the region around $\Delta Bt>1K$ pixels is let to the user's estimate. This recommendation allows for several possible mis-interpretation scenarios. In the following, we have discarded pixels with an associated $\Delta Bt <0.4K$ while we investigated using the $\Delta Bt>1K$ as flag [see Section 2.2.1]

2.1.2 Volcanic SO_2 sources

In order to assess the IASI/Metop CDR SO_2 VCDs, a number of volcanic eruptions were chosen, enumerated in Table 1. In the following document, a number of these eruptions will be used to

demonstrate the various aspects of the dataset as well as in the validation against the correlative dataset, that of S5P/TROPOMI.

Table 1. Selected volcanic emissions studied within this work.

Starting day	Ending day	Name	Country
20071003	20071007	JebelalTair	Yemen
20080511	20080514	Etna	Italy
20080718	20080719	Okmok	Alaska
20080811	20080906	Kasatoschi	Alaska
20081105	20081112	Dalafilla	Ethiopia
20090619	20090716	Sarychev	Russia
20100515	20100520	Eyjafjallajoekull	Iceland
20110523	20110604	Grimsvotn	Iceland
20110618	20110627	Nabro	Eritrea
20111105	20111117	Niryacongo	Congo
20121223	20121231	Copahue	Chile
20140214	20140222	Kelut	Indonesia
20150422	20150430	Calbuco	Chile
20160102	20160115	Soputan	Indonesia
20160326	20160330	Pavlov	Alaska
20180219	20180228	Sinabung	Indonesia
20180626	20180702	SierraNegra	Ecuador
20180726	20180802	Ambae	Vanuatu
20190622	20190715	Raikoke	Russia
20200112	20200115	Taal	Philippines
20211219	20211231	HungaTonga	Tonga

2.2 Inter-sensor investigations

In the following section we first investigate the effect of the recommended filtering of the IASI/Metop CDR as well as the inter-sensor consistency of the two instruments.

2.2.1 Investigation on the ΔBt flag

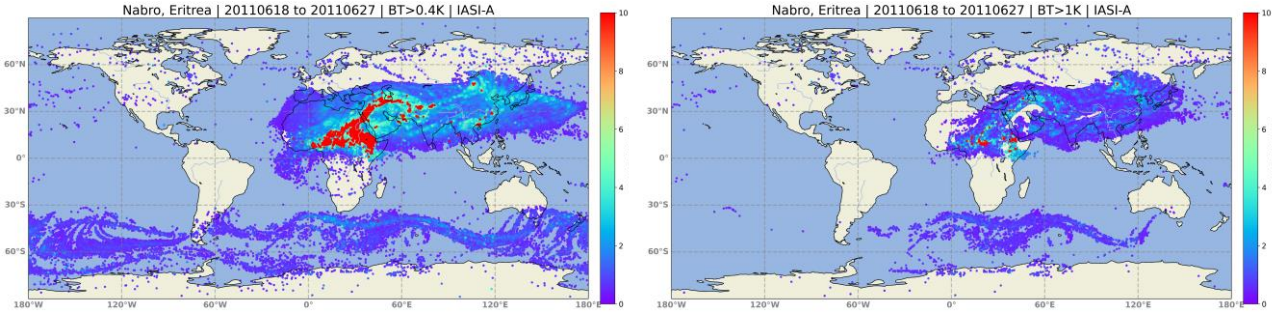

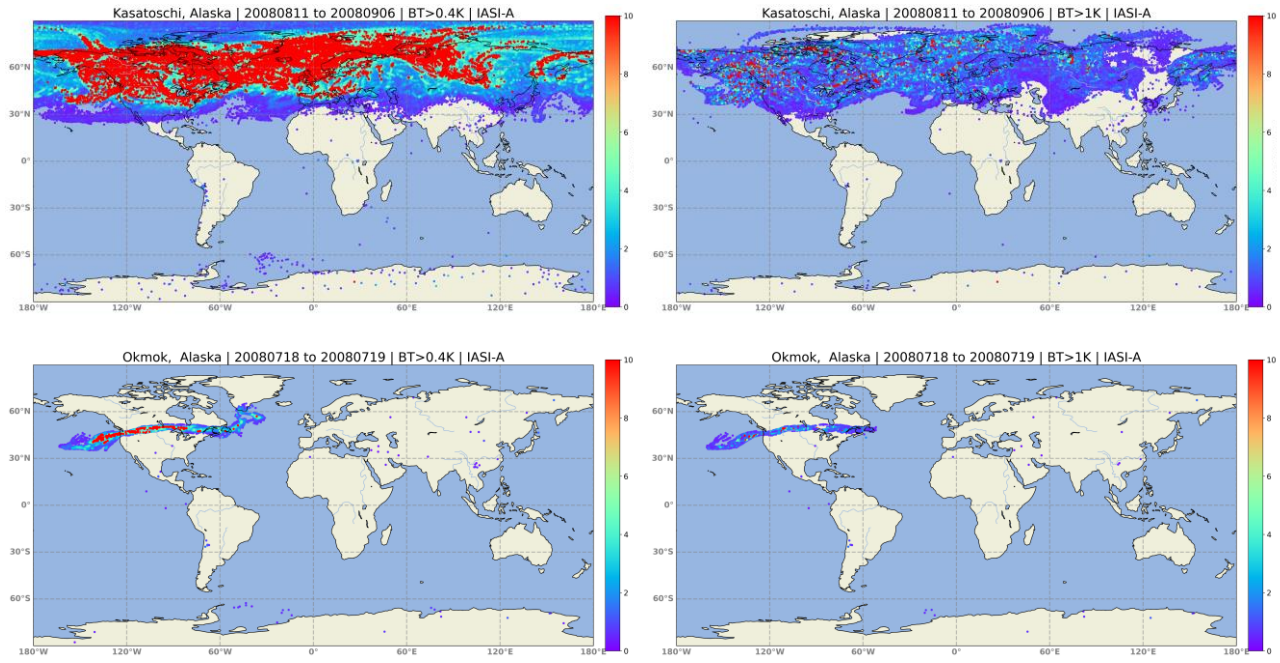

Figure 1. The effect of the ΔBt recommended cut-off on the IASI SO_2 reported loads for three major eruptions during the IASI-A timeline. Left column, ΔBt > 0.4K and right column, ΔBt > 1K.

As discussed in Section 2.1.1, there exist a recommendation that pixels with associated ΔBt > 0.4K should be used if in the vicinity of pixels with associated ΔBt > 1K. The extend of this vicinity is left to the user to define. To begin with, we show in Figure 1, the effect of applying a ΔBt > 1K in the entire dataset [right column] on three major eruptions during the IASI-A timeline. All eruptive days are simply plotted overlain, without any gridding, sorted per SO_2 load so that the highest loads appear in the plot. In all cases, a number of high SO_2 loads are filtered out by the strict filter of ΔBt > 1K.

For both cases, however more pronounced for the Kasatochi eruption shown in the upper row of Figure 1, numerous high SO_2 loads are excluded when using the stricter filtering. We overall consider the recommendation of "choosing a vicinity" beyond the typical abilities of the standard user of satellite data and **would suggest that a flag pointing to such occurrences be included in future versions of the dataset**. The ACSAF GOME2/Metop SO_2 product (Valks et al., 2019) includes such a volcanic flag and a similar approach could be applied to the IASI/Metop SO_2 products.

2.2.2 Inter-sensor consistency

The inter-sensor consistency is examined using known volcanic eruptions during the tandem period of operations of the two instruments. In Figure 2, two such examples are presented for the Ambae, 2018 eruptive period [upper] and the Kelut, 2014, eruptive period [lower]. The locations and spreads of the plumes coincide to a significant degree, also demonstrated in the form of histogram representations of the SO_2 loads in Figure 3.

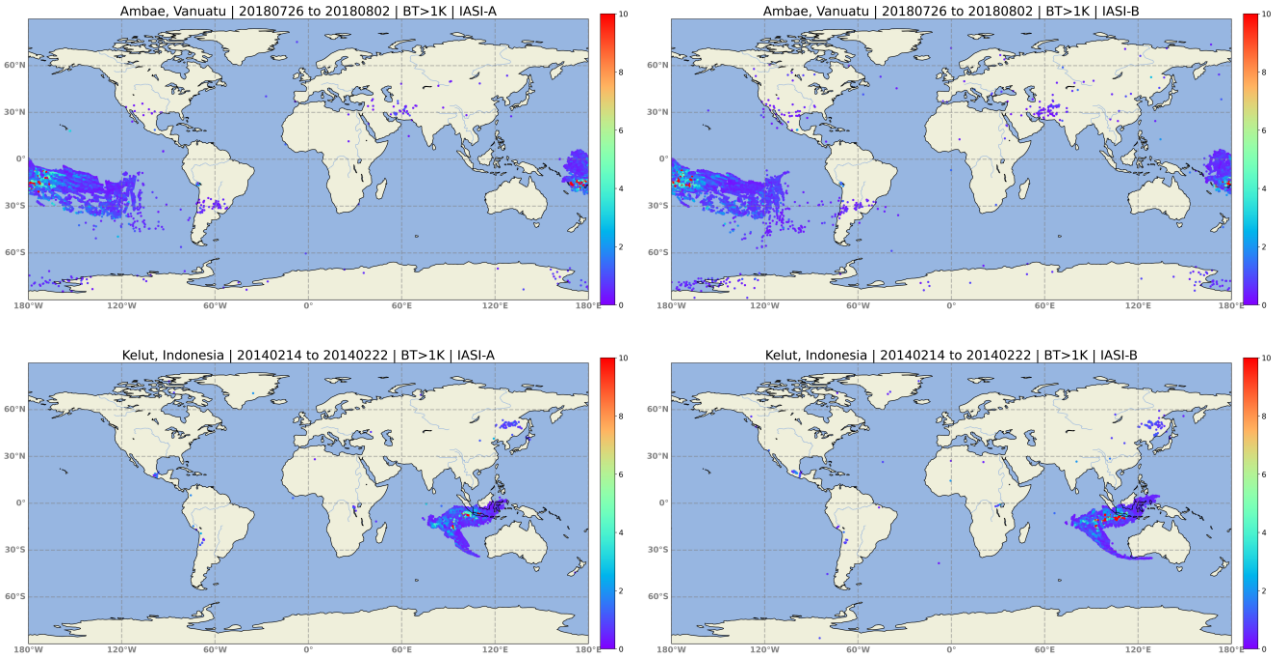

Figure 2. The IASI-A [left] and IASI-B [right] ΔBt > 1K SO_2 loads during the Ambae, 2018 eruption [upper] and the Kelut, 2014 eruption [lower].

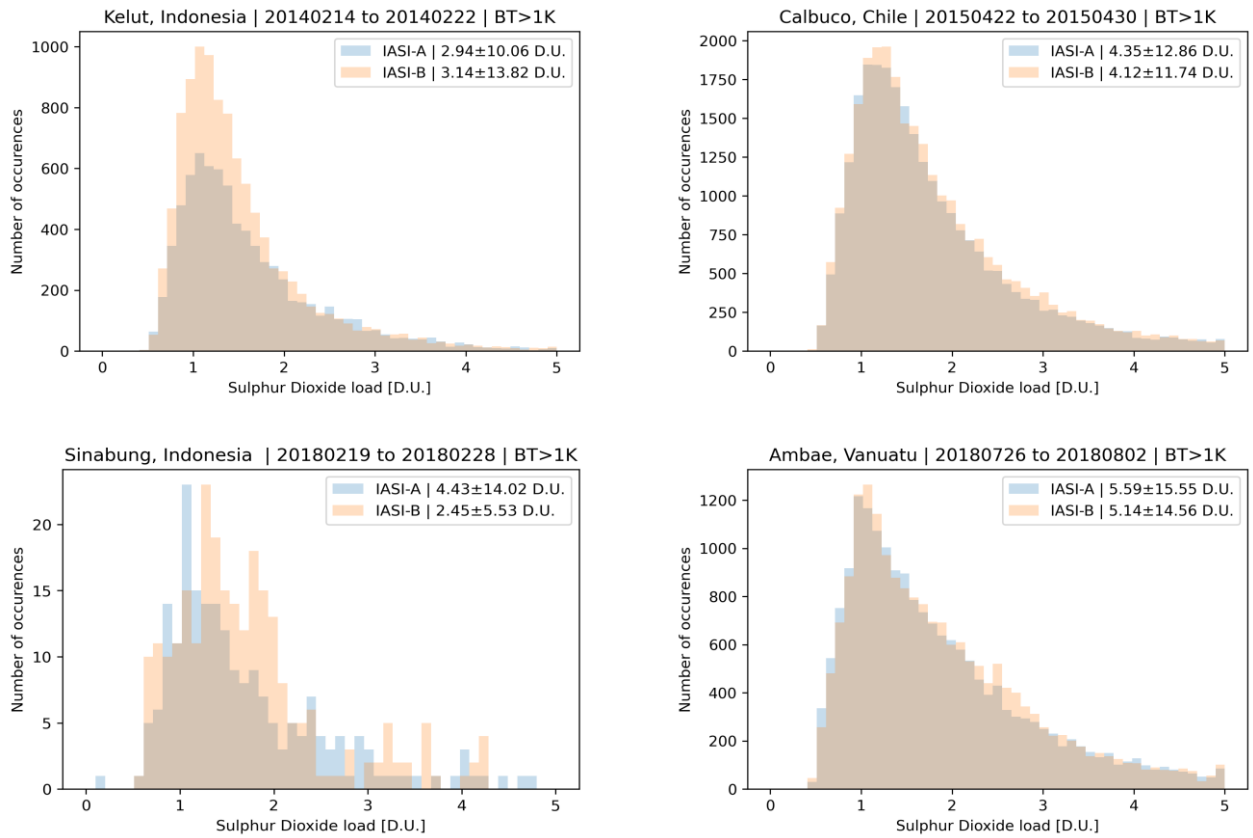

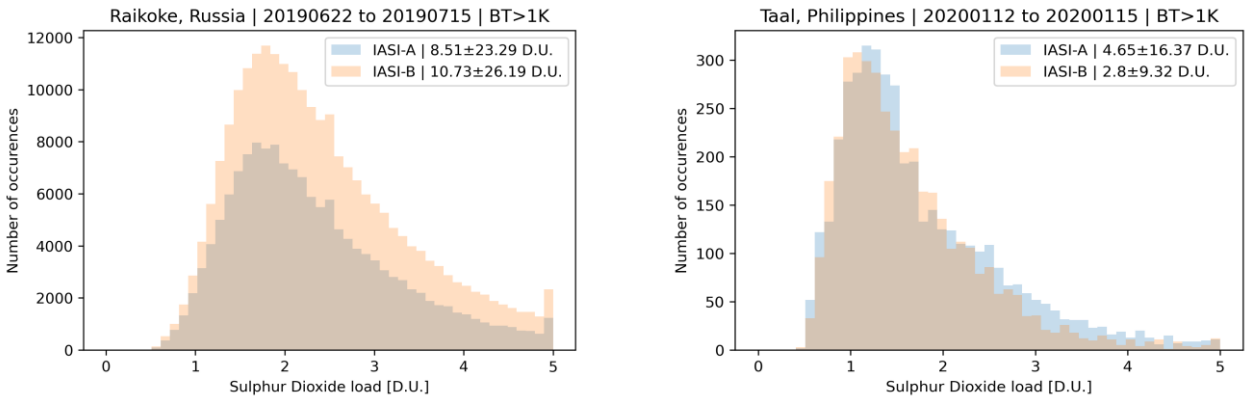

Figure 3. Histograms of the IASI-A [blue] and IASI-B [orange] ΔBt > 1K SO_2 loads during six concurrent volcanic eruptions between 2014 and 2020 in temporal sequence. Names and time periods are insert in the titles.

In Figure 3, histograms of the IASI-A [blue] and IASI-B [orange] ΔBt > 1K SO_2 loads during six concurrent volcanic eruptions between 2014 and 2020 are presented. The eruptions were chosen on purpose so as to identify possible issues that may affect users. The timelines of the eruptive days are shown in each title and the mean loads and 1-sigma deviation in the figure legend. The first issue to note is that differences appear to exist for the Kelut eruption [upper left], the Sinabung [middle left] and the Raikoke eruption [bottom left], which however are due to a few missing IASI-A days from the timeline. The second issue affects the Taal [bottom right] eruptions where both sensors reported data during all four eruptive days. However IASI-A reports a number of pixels with high SO_2 load which are either not sensed by IASI-B, or do not pass the recommended flag filtering or do not pass the ΔBt > 1K flag. This results in the difference in mean loads presented in this case. Finally, during eruptions were neither of these issues are present, such as during the Calbuco [upper right] and Ambae [middle right] eruptions, the mean loads and distributions between the two sensors are in agreement within the first decimal place.

We hence conclude that the **IASI-A and IASI-B SO_2 CDR datasets can be merged and used in tandem**, when the user prefers to increase the collocations, always considering the time difference of the two observations.

3. SULPHUR DIOXIDE COLUMN VALIDATION

In this section, comparisons of the IASI/Metop CDR SO_2 columns are presented against collocated satellite estimates by S5P/TROPOMI and ground-based estimates by BIRA MAX-DOAS systems.

3.1 Validation against S5P/TROPOMI

The TROPOMI sensor on board the Sentinel-5P platform samples the Earth's surface with a revisit time of one day and a spatial resolution of 5.5x3.5 km^2 since August 2019. This allows the resolution of fine details of SO_2 plumes and S5P is arguably a valuable tool in anthropogenic SO_2 emissions studies but also volcanic emissions, from degassing to eruptive processes. The SO_2 retrieval algorithm is based on the DOAS technique and is fully described in the relevant ATBD [Theys et al., 2022] as well as in Theys et al., 2017, where additional verification results as part of the algorithm development are also presented. The S5P/TROPOMI SO_2 dataset is publicly available via the Copernicus Open Access Hub, Sentinel-5P Pre-Operations Data Hub (copernicus.eu). In the following, offline data between 01.05.2018 and 31.12.2019, versions 01.01.05 and 01.01.06, were downloaded. As suggested in the ReadMe file[1], in case of volcanic emissions the only filtering criteria required is that the solar zenith angle is < 70° and the sulfur dioxide detection flag to be raised. The S5P/TROPOMI volcanic SO_2 at an assumed 7km plume was gridded on a 0.25x0.25 degree grid on a daily basis. In Figure 4, the daily SO_2 load (D.U.) for three major eruptions, Sierra Negra and Ambae, in 2018, and Raikoke, in 2019 is shown on the left, and the equivalent IASI-A fields on the right column.

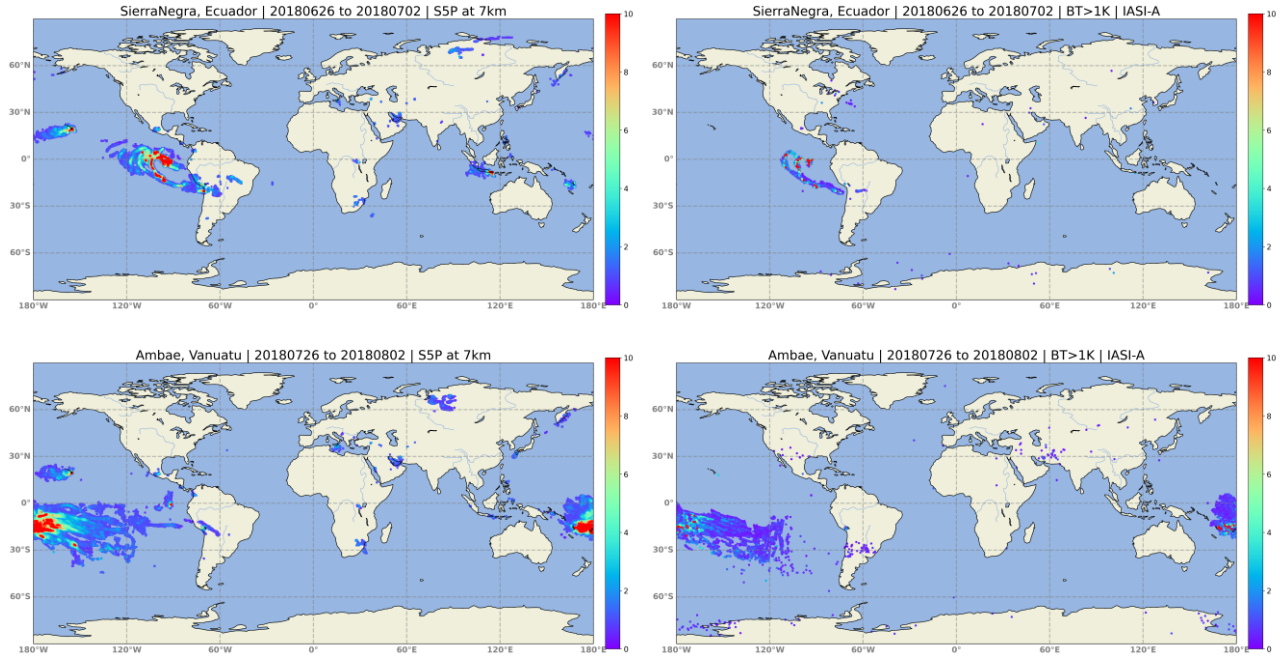

[1] https://sentinels.copernicus.eu/documents/247904/3541451/Sentinel-5P-Sulphur-Dioxide-Readme.pdf

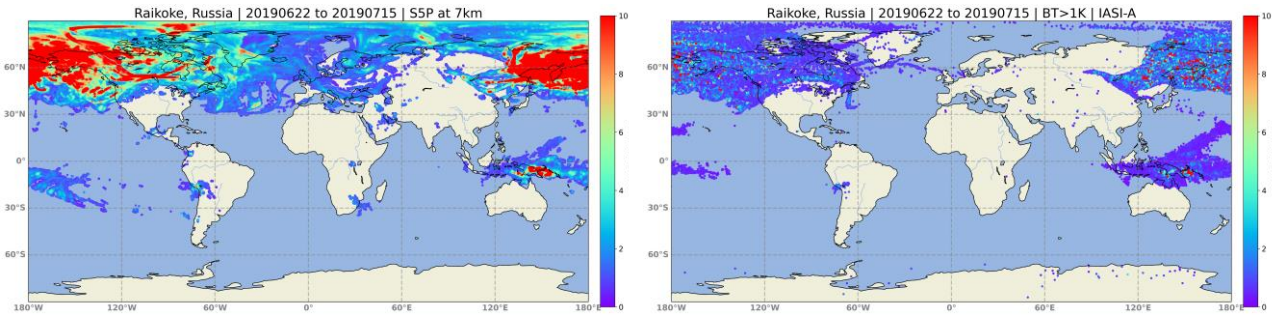

Figure 4. S5P daily volcanic SO_2 VCD at 7km for three major eruptions, Sierra Negra and Ambae, in 2018, and Raikoke, in 2019 shown on the left column and the IASI-A ΔBt> 1K observations for the same eruptions on the right column.

In Table 2, the mean volcanic SO_2 loads per eruption between S5P, IASI-A and IASI-B (where applicable) are provided for the three eruptions shown in Figure 4. Overall, the mean IASI SO_2 loads report higher values, and a far higher variability – denoted by the 1-sigma of the mean – than the S5P SO_2 loads. The IASI-A and -B maxima are also far larger than the equivalent ones for S5P which led us to proceed in calculating the SO_2 masses in ktons/day, as a more representative comparative metric.

Table 2. Comparison of the mean SO_2 load per eruption between S5P, IASI-A and IASI-B.

	S5P at 7km [D.U.]			**IASI-A [D.U.]**			**IASI-B[D.U.]**		
	min	max	mean±std	min	max	mean±std	min	max	mean±std
Sierra Negra	0.32	171.3	1.9±3.28	0.2	227.0	14.03±32.17	n/a	n/a	n/a
Ambae	0.34	195.0	2.16±4.11	0.2	250.0	5.11±16.52	0.2	314.0	4.22±14.13
Raikoke	0.29	802.0	2.98±8.26	0.2	1658.0	6.24±22.17	0.1	1581.0	6.8±22.6

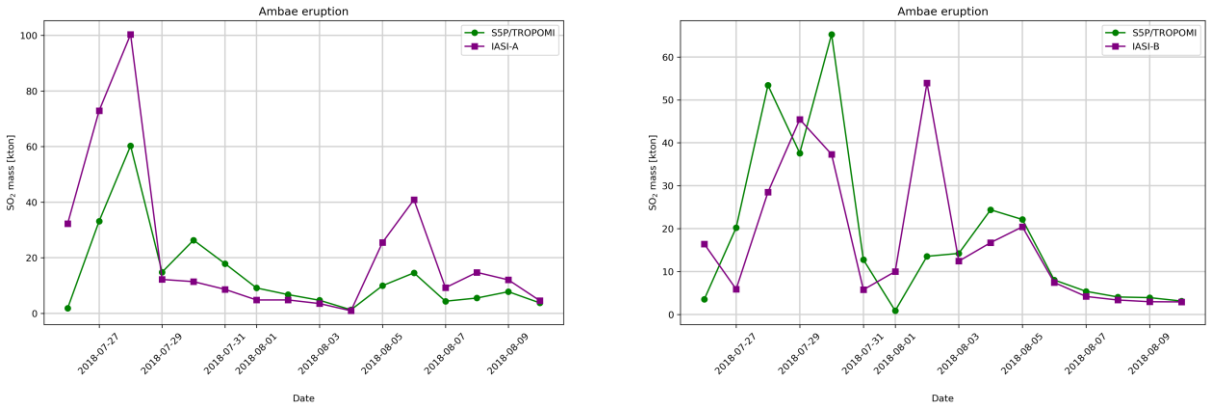

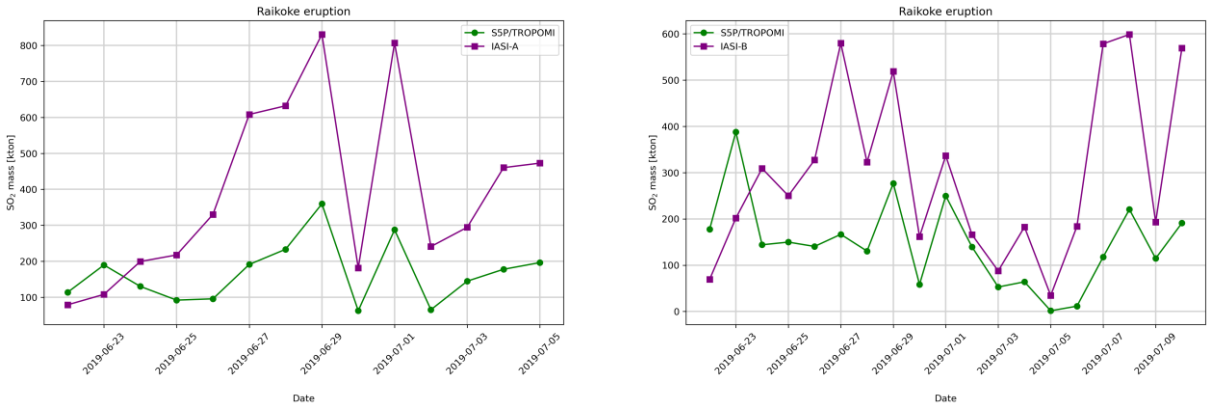

Figure 5. Same-pixel comparison of SO_2 mass [kt/day] for the Ambae [upper] and the Raikoke [lower] eruptions between S5P and IASI-A [left] and IASI-B [right].

In Figure 5, the collocated pixels between S5P and IASI-A [left] and IASI-B [right] were used to calculate the SO_2 masses in kt/day emitted after the Ambae 2018 (upper) and Raikoke 2019 (lower) eruptions. The two sensors report a nice co-variability in the days following the eruptions, with IASI reporting higher loads, as expected when considering the SO_2 loads shown in Table 2.

3.2 Comparisons against the MAX-DOAS network

Several BIRA-IASB stations (http://uv-vis.aeronomie.be/groundbased/stations) cover part of the available datasets time-period (2007-2021, see Table 3) and the IASI SO_2 data have been extracted in a radius of 300km around these sites, as shown in Figure 6 for the IASI-A data and in Figure 7 for the IASI-B data.

As illustrated in Figure 6 for IASI-A, the overpasses have been calculated keeping all the valid points (i.e., points with $\Delta Bt > 0.4K$) and then a stricter filtering applying the recommended $\Delta Bt > 1K$ threshold to only highlight the volcanic cases. As discussed in Section 2.2.1 a recommendation on using pixels with associated $\Delta Bt > 0.4K$ if in the vicinity of pixels with associated $\Delta Bt > 1K$ exist but is not implemented by default and is left to the users to apply it. We will test the impact of this choice in a few cases below.

When applying the filter on $\Delta Bt > 1K$, several SO_2 plumes from large eruptions can be seen over several BIRA-IASB stations, with several plumes travelling around the Northern and/or Southern hemispheres for several days, such as:

- the Kasatochi eruption in August 2008 (Clarisse et al., 2012), which travelled around the northern hemisphere between 11/08/2008 and 06/09/2008;

- the Sarychev eruption on the 30/6/2009;

- the Eyjafjallajokull eruption on the 17/5/2010;

- the Nabro eruption between the 12 and 28 June 2011 (Clarisse et al., 2014);

- the Grimsvotn eruption at the end of May/early June 2011;

- the Nyamuragira eruptive period between 6/11/2011 and 6/12/2011;

- the Raikoke eruption in late June 2019;

- the Ubinas eruption on the 23/7/2019.

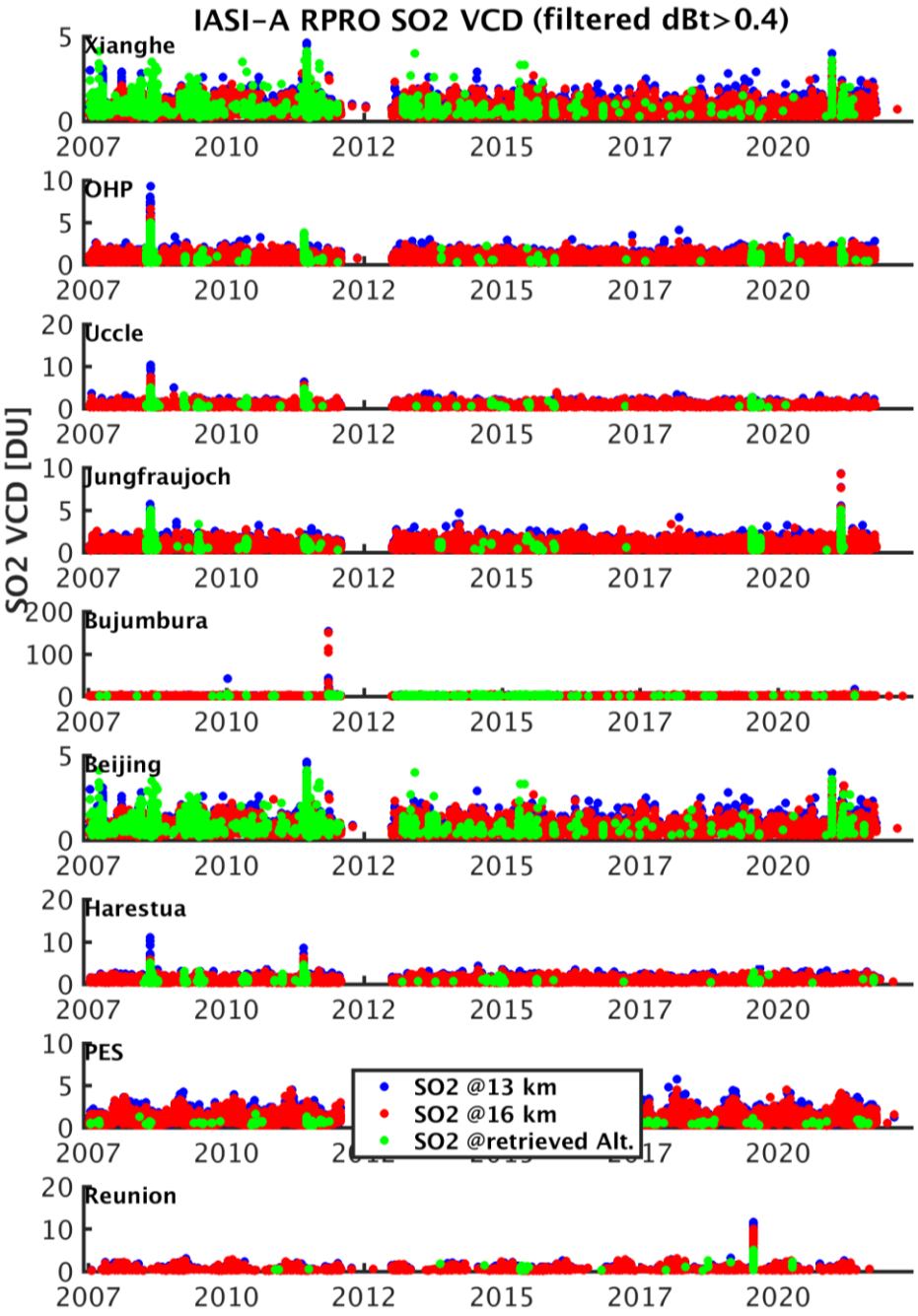
IASI-A RPRO SO2 VCD (filtered dBt>0.4)
SO2 VCD [DU]
Xianghe
OHP
Uccle
Jungfraujoch
Bujumbura
Beijing
Harestua
PES
Reunion
SO2 @13 km
SO2 @16 km
SO2 @retrieved Alt.
2007
2010
2012
2015
2017
2020

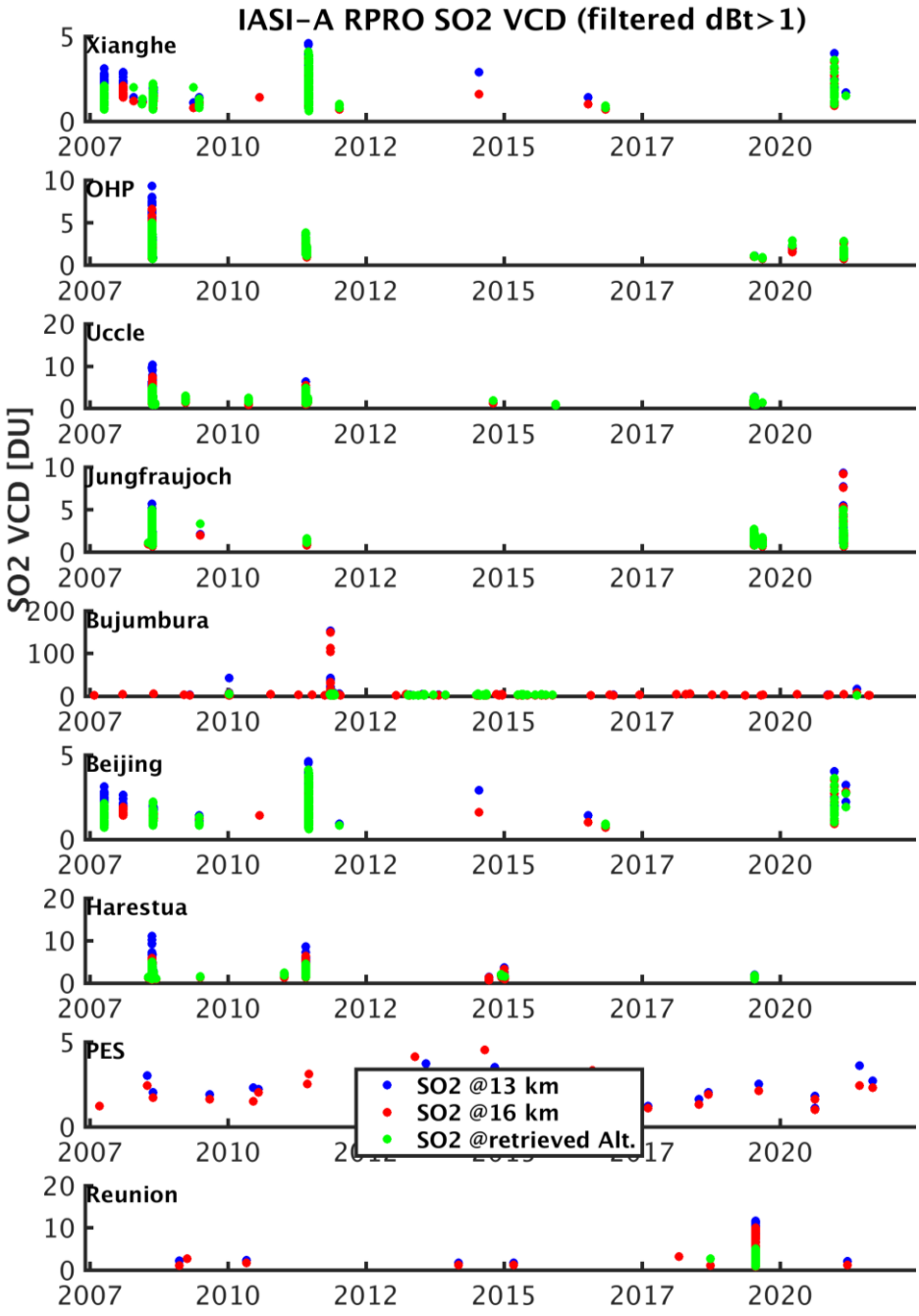

Figure 6.IASI-A SO_2 columns overpasses around the BIRA-IASB stations; SO_2 VCD estimates for 13km (blue dots), 16km (red dots) and for the retrieved height (green dots). Two filtering cases are shown, for $\Delta Bt > 0.4K$ (top) and $\Delta Bt > 1K$ (bottom).

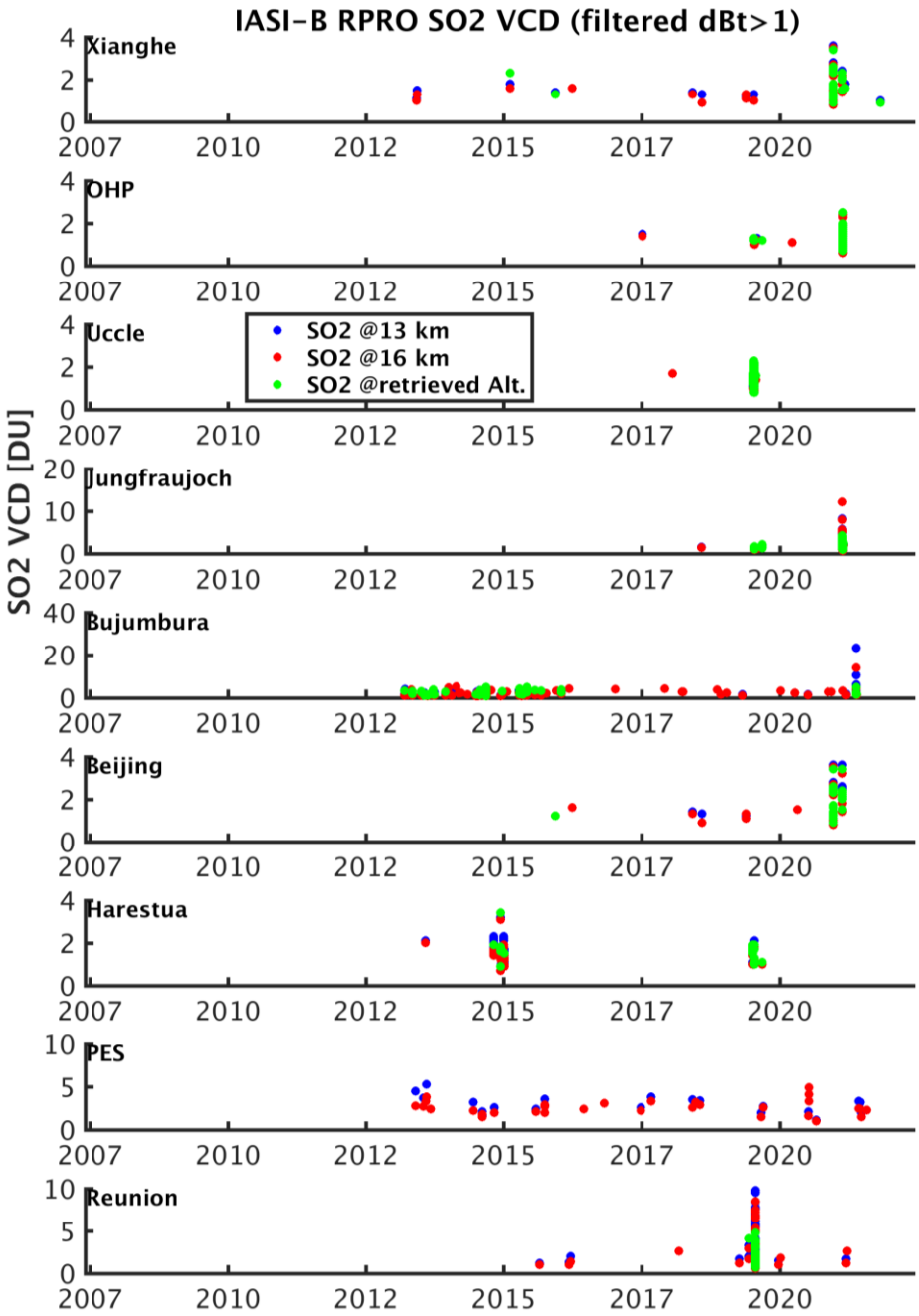

Figure 7. IASI-B SO_2 columns overpasses around the BIRA-IASB stations for $\Delta Bt > 1K$; SO_2 VCD estimates for 13km (blue dots), 16km (red dots) and for the retrieved height (green dots).

Table 3. Information on BIRA-IASB sites, with relevant details for SO_2 retrievals possibilities.

Station	Full measurement period	Information relevant for SO_2
Uccle (50,5°N, 4°E, **Belgium**)	mini-MAXDOAS instrument from 5/2011 to 2/2016 (Gielen et al., 2014) and a new MAXDOAS instrument from 2/2017 to 2/2020 (Dimitropoulou et al 2020; 2022)	
Jungfraujoch (46.5°N, 7.98°E, **Switzerland**)	ZenithSky geometry since the '90 with a SAOZ, a MAXDOAS geometry from 7/2010 to 10/6/2019 (Hendrick et al, 2012) and a new Zenith (only VIS) since 3/2022	The MAXDOAS UV channel had permanent failure in mid-June 2019
OHP (44°N, 7.71°E, **France**)	MAXDOAS geometry from 2005 to March 2017 (Valks et al., 2011)	measuring in the spectral region from 323-390nm and is thus not covering the SO_2 analysis region (305-317.5nm)
Xianghe (39.75°N, 116.96°E, **China**)	MAXDOAS from 2010 to summer 2022 (Clémer et al., 2010; Hendrick et al, 2014)	instrumental problem between 7/2018 to 10/2019 (measuring only in zenith mode). The UV channel had permanent failure in end October 2021.
Bujumbura (3°S, 29°E, **Burundi**)	MAXDOAS from 11/2013 to mid 2017 (Gielen et al., 2017)	Problem with UV channel between 25/4/2014 and 14/4/2015 and since 16/8/2017.
Reunion (21°S, 55°E, **Reunion Island**)	MAXDOAS in LePort from 4/2016 to 1/2018 and on Maido since 6/2018	Problem with the degradation of the UV slit function since mid of 2021. Data not usable after.

Shown in the previous figures and considering the ground-based measurements limitations (as discussed in Table 3), five stations have at least one interesting eruption to look into in detail. Ground-based SO_2 analysis are not performed routinely, and only the time-periods with strong volcanic SO_2 signals revealed by both IASI and GOME2 observations are analysed.

The ground-based spectra have been analysed using the DOAS settings specified in Wang et al., 2014 (analysis in the 305-317.5 nm window) with a fixed reference spectrum close to the period of interest (on a day not affected by the eruption). The slant columns measured at zenith mode are used to

estimate the stratospheric SO_2 content by using a geometrical stratospheric AMF that depends only on the solar zenith angle (Honninger et al., 2004):

$$AMF_{strato} = 1/\cos(SZA) \quad (1)$$

For large stratospheric eruptions, such as Kasatochi, Grimsvotn, Nabro, etc. (Carn et al., 2016 and Hopfner et al., 2015), both MAXDOAS and ZenithSky instruments are sensitive to the SO_2 in the stratosphere, and the stratospheric SO_2 content is obtained as:

$$VCD_{strato} = DSCD_{zenith}/AMF_{strato} \quad (2)$$

In the following sub-sections, the different comparison cases for the stations listed in Table 3 are presented.

Uccle

An illustration of the IASI-A and IASI-B overpasses for Uccle is given in Figure 8 for the whole timeline on top and for two specific periods in 2011 for IASI-A and 2019 for IASI-B at the bottom.

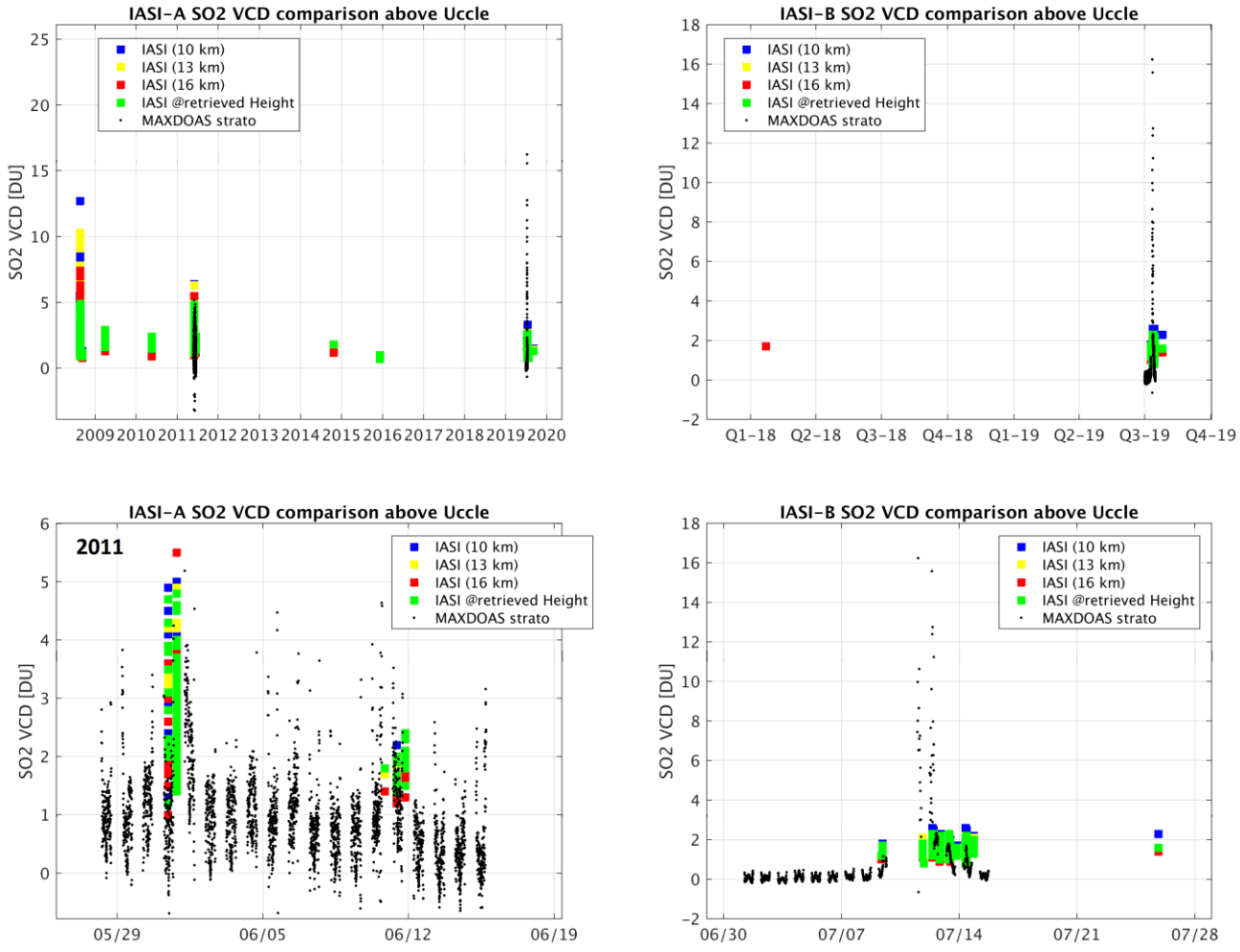

Figure 8. Uccle SO_2 VCD time-series of the IASI-A and IASI-B overpasses (colored squares) and the analyzed ground-based data (black dots). Top: the whole time-series; Lower Left: June 2011 Grimsvotn eruption; Right: July 2019 Raikoke eruption.

The Uccle station can be challenging because the instrument measuring in the 2011-2016 period is a commercial mini-MAXDOAS system from Hoffmann (Gielen et al., 2014) and the SO_2 retrieval is quite noisy. From 2/2017 to 2/2020 a scientific grade MAXDOAS was measuring in Uccle, and the noise on the SO_2 is much reduced. We analysed the May-June 2011 and the July 2019 periods for the Grimsvotn and the Raikoke eruptions from these instruments.

Two days in 2011 with IASI-A SO_2 collocations are shown in Figure 8 are illustrated in Figure 9 (31/5, left and 11/6, right). On the 31/5/2011 IASI-A only has pixels within 80km with ΔBt>1K in the nighttime overpass and that on the 11/06/2011 all the pixels are quite far away from the stations, at about 150 to 250km. The distance of the satellite pixel from the ground-station is shown as the colour of the satellite circles, with the ground-based assessment shown in red.

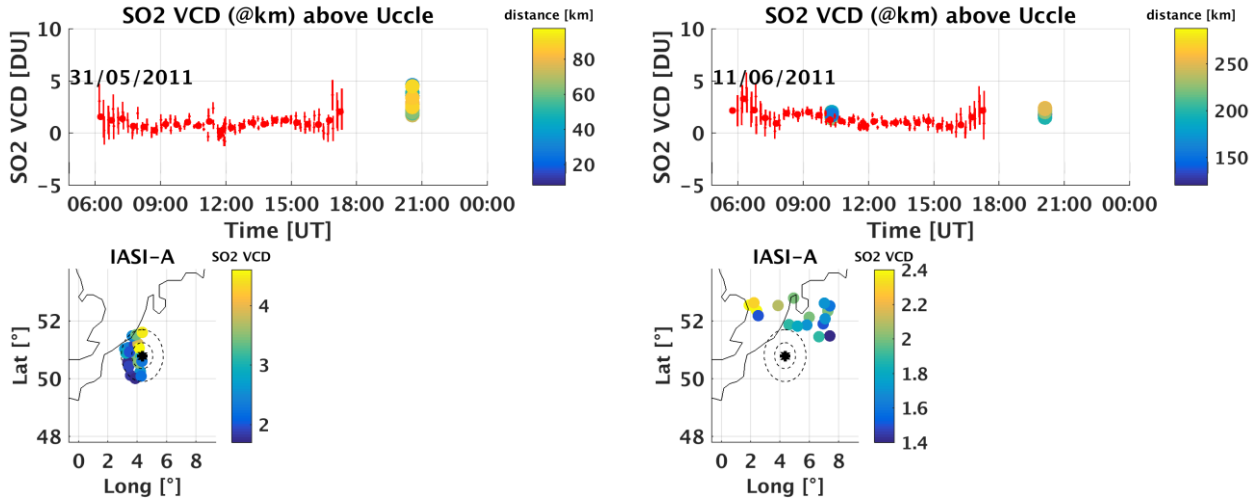

Figure 9. SO_2 VCD comparisons at Uccle for 2 days focusing on the Grimsvotn eruption in 2011, left and right columns. Each figure contains an upper panel with the SO_2 VCD time-series from the zenith measurements (in red) and from IASI (columns at the retrieved height, color-coded as a function of the station distance). The lower panel presents the geographical distribution of the IASI SO_2 VCD around the station (circles at 50km and 100km are plotted in dotted lines).

The few days with existing IASI-B SO_2 height seen in Figure 8 for 2019, are illustrated in Figure 10, keeping only the pixels that are within 80km of the Uccle site. IASI-A collocations are also available here. It can be seen that:

- On the first day (9/7/2019, show in the upper left), only IASI-B has some volcanic SO_2 pixels (with ΔBt>1K), and there is a tendency of increasing SO_2 during the morning.
- On the 12th of July 2019 (upper right) there are no temporal collocations, but IASI-A and IASI-B have volcanic signals in both the day and night overpasses, with similar SO_2 levels than the ground-based data, and with a tendency of larger columns in the night-time overpass, as for the growing SO_2 columns during the day.
- On the 13th and 14th July (bottom row), both IASI-A and IASI-B day overpasses are in agreement with the ground-based data, with values of about 2DU and with slightly larger values for IASI-A compared to IASI-B and a decreasing SO_2 load during the day.

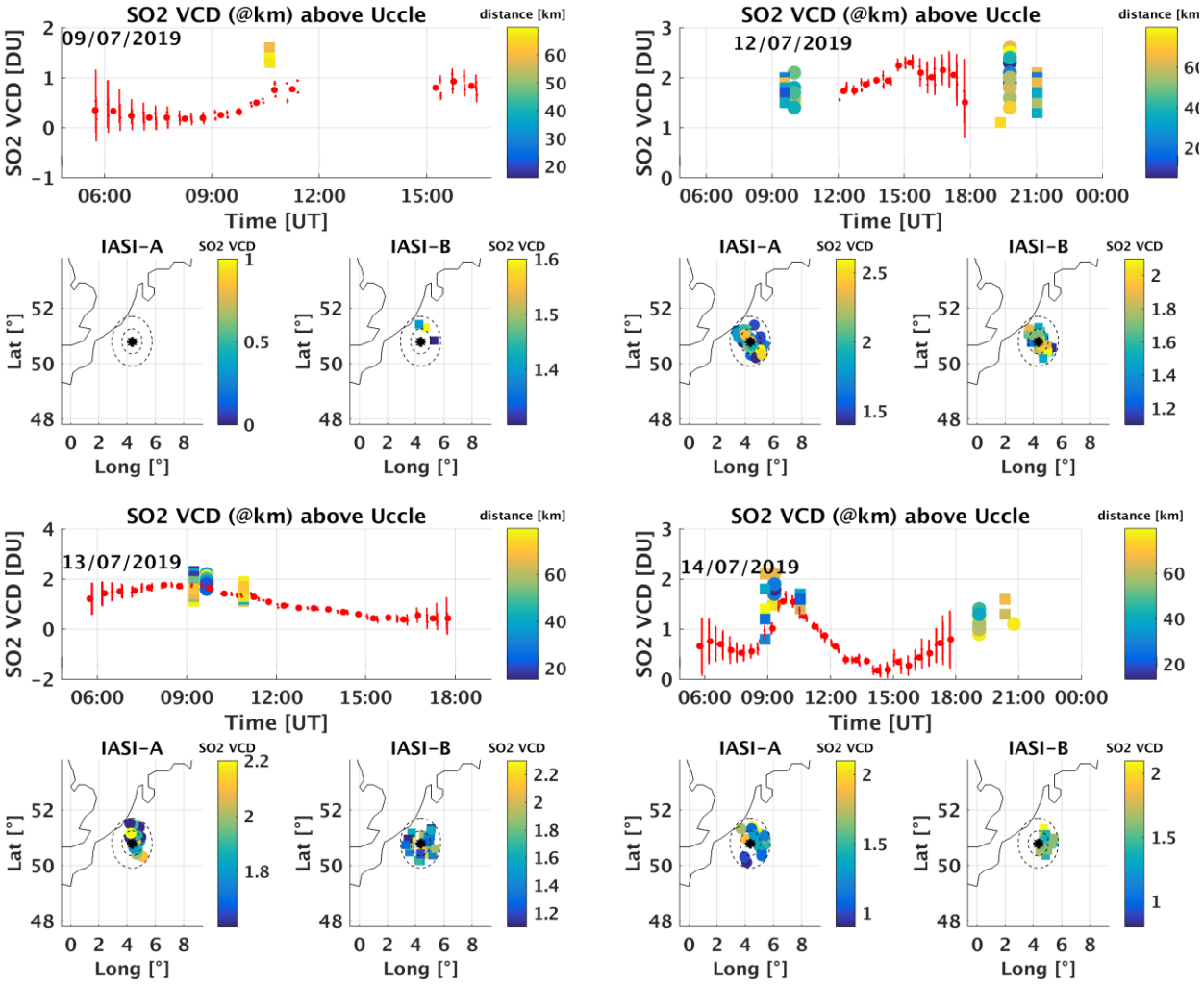

Figure 10. SO_2 VCD comparisons at Uccle focusing on the July 2019 eruption (Raikoke). Days are left to right, top to bottom. Each panel present an upper panel, with the SO_2 VCD time-series from the zenith measurements (in red) and from IASI (columns at the retrieved height, color-coded as a function of the station distance; circles for IASI-A, squares for IASI-B). The second panel presents the geographical distribution of the IASI-A (left) and IASI-B (right) SO_2 VCD around the station (circles at 50km and 100km are plotted in dotted lines).

Jungfraujoch

An illustration of the IASI-A and IASI-B overpasses for Jungfraujoch is given in Figure 11 for the whole time-series in the upper row and for June 2011 and in spring/summer 2019 when the Grimsvotn and the Raikoke plumes circulated around the Northern Hemisphere in the bottom row. As it can be seen, on the 6 of June 2011 there is an SO_2 enhancement for both ground-based and IASI-A, while unfortunately the MAXDOAS UV channel stopped measuring on 10th June 2019, so there is no possibility to compare for the 2019 case and later. During the Kasatochi eruption (August 2008) only the BIRA SAOZ was measuring (MAXDOAS installed in 2010), which is not measuring in the SO_2 region.

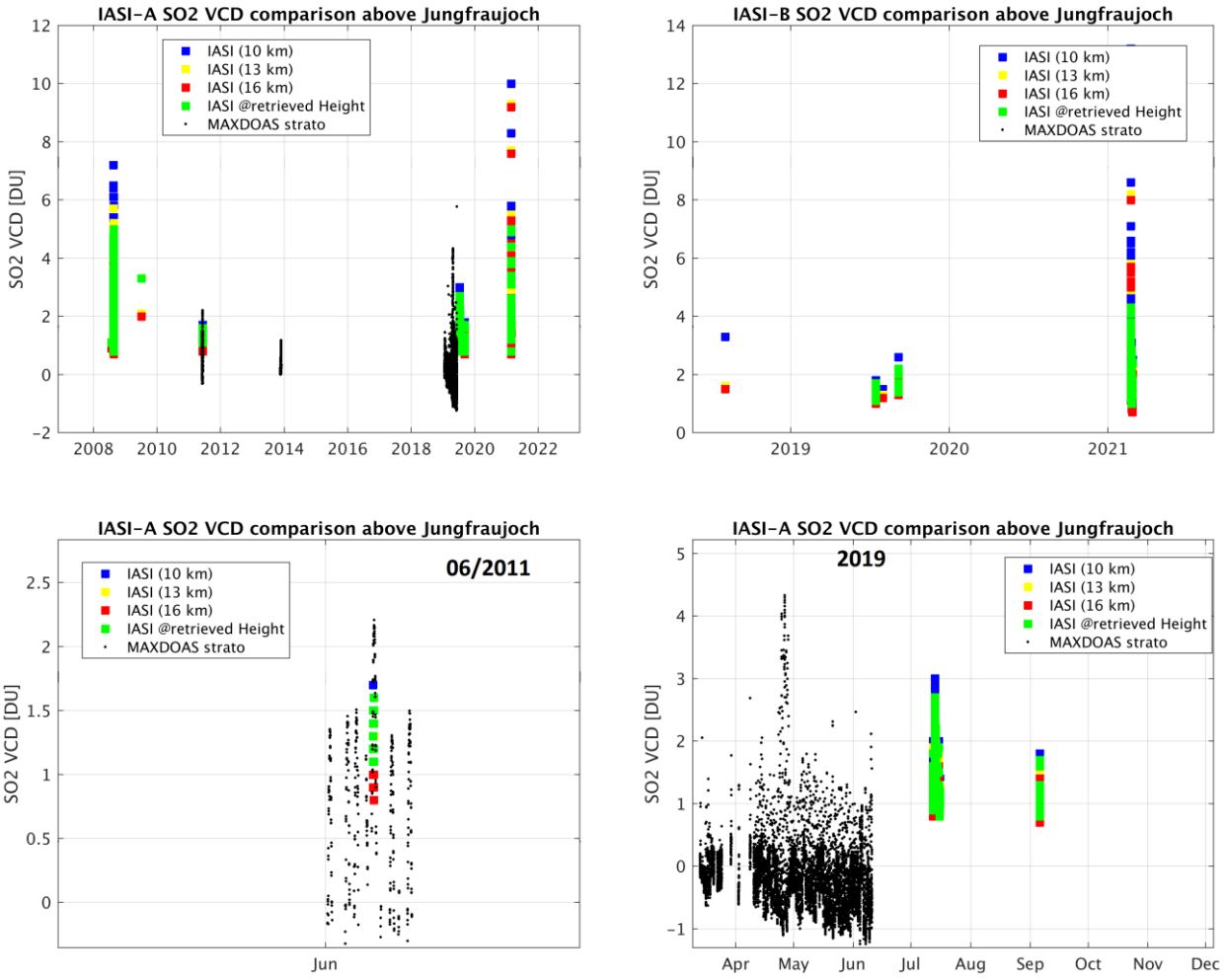

Figure 11. Jungfraujoch SO_2 VCD time-series of the IASI-A (left) and IASI-B (right) overpasses (colored squares) and the analyzed ground-based data (black dots). Up: the whole 2007-2021 time-series; Bottom left: zoom on June 2011 for the Grimsvotn eruption; Bottom right: zoom on summer 2019 for the Raikoke eruption.

The case of 6 June 2011 is shown in detail in Figure 12, with one IASI-A pixel with $\Delta Bt > 1$ K in the 80km around the site. The satellite SO_2 estimate is very close to the value observed from the ground for that day.

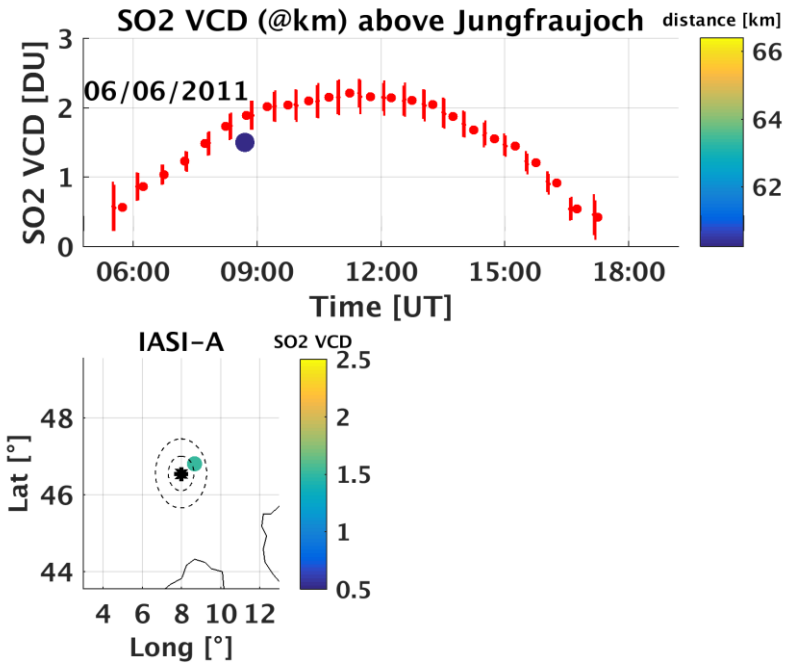

Figure 12. SO_2 VCD comparisons at Jungfraujoch on 6/6/2011 for the Grimsvotn eruption. The figure presents an upper panel, with the SO_2 VCD time-series from the zenith measurements (in red) and from IASI-A (SO_2 columns at the retrieved height, color-coded as a function of the station distance). The lower panels present the geographical distribution of the IASI-A SO_2 VCD around the station (circles at 50km and 100km are plotted in dotted lines).

In the [VR], the ground-based data at the end of 2013 revealed a volcanic plume that was also observed by the IASI-A SO_2 AERIS dataset, coming from an Etna plume from an eruption on the 23rd of November travelling north and reaching Jungfraujoch on the 24/11/2013. This eruption is not retained by the ΔBt>1K selection, but we can find it when looking at the IASI pixels with ΔBt>0.4K, as illustrated in Figure 13.

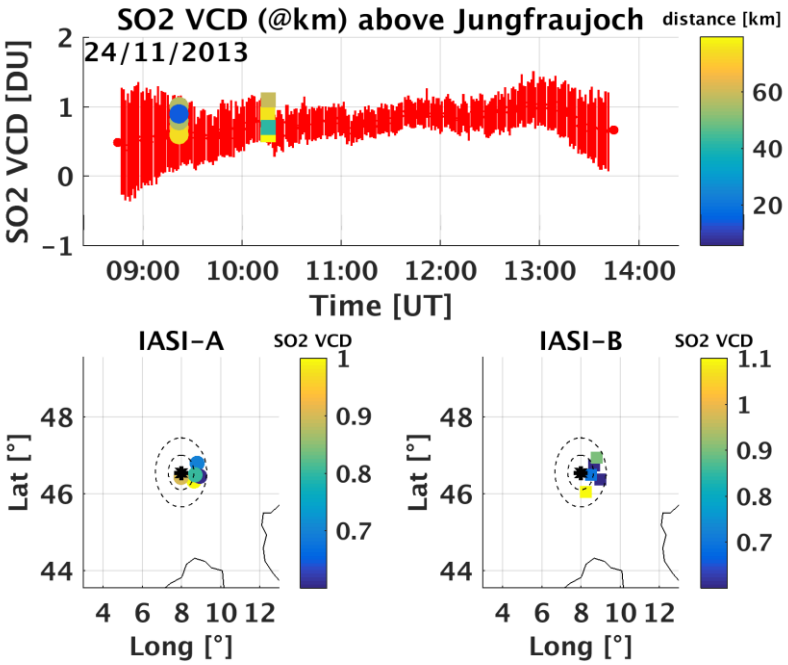

Figure 13. SO_2 VCD comparisons at Jungfraujoch on 23/11/2013 for an Etna eruption. The figure presents an upper panel, with the SO_2 VCD time-series from the zenith measurements (in red) and from IASI-A (circles) and IASI-B (squares) (SO_2 columns at the retrieved height, color-coded as a function of the station distance, for all pixels with **ΔBt>0.4K** within 80km of the station). The lower panels present the geographical distribution of the IASI-A SO_2 VCD around the station (circles at 50km and 100km are plotted in dotted lines).

Bujumbura

An illustration of the IASI-A overpass for Bujumbura is given in Figure 14 for the whole time-series in the left plot and for the November 2011 Nyamuragira eruption in the right. It can be seen that the very high SO_2 VCD estimated for plume altitudes between 10 to 16km are in fact reduced to up to ~4DU when the retrieved SO_2 height is used as information for the SO_2 VCD estimation. The MAXDOAS data only measured during the period 11/2013 to mid-2017, so this big eruption is not covered.

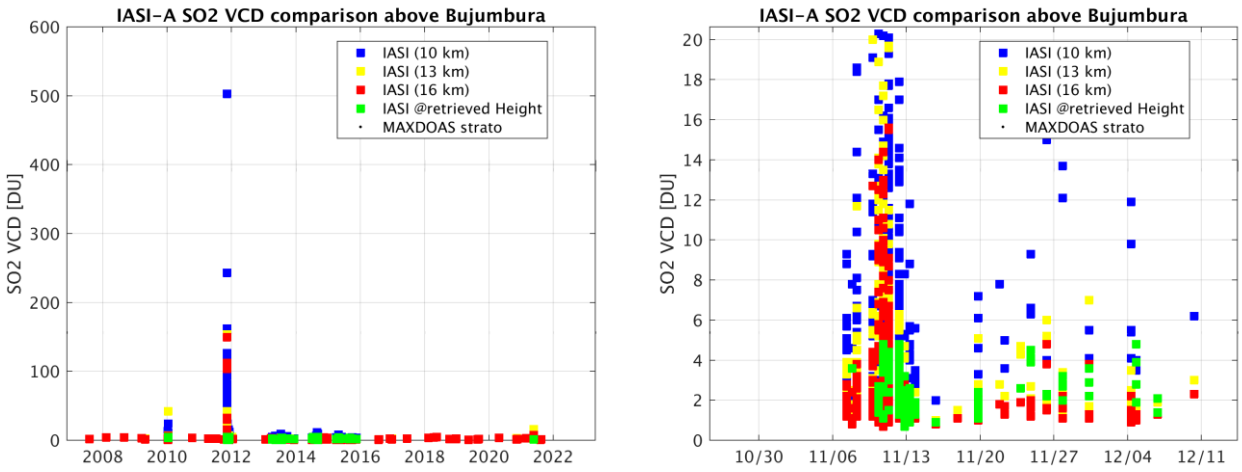

Figure 14. Bujumbura SO_2 VCD time-series of the IASI overpasses (colored squares). Left: the whole 2007-2021 time-series; right: zoom on Nyamuragira eruption of 6/11 to 6/12/2011.

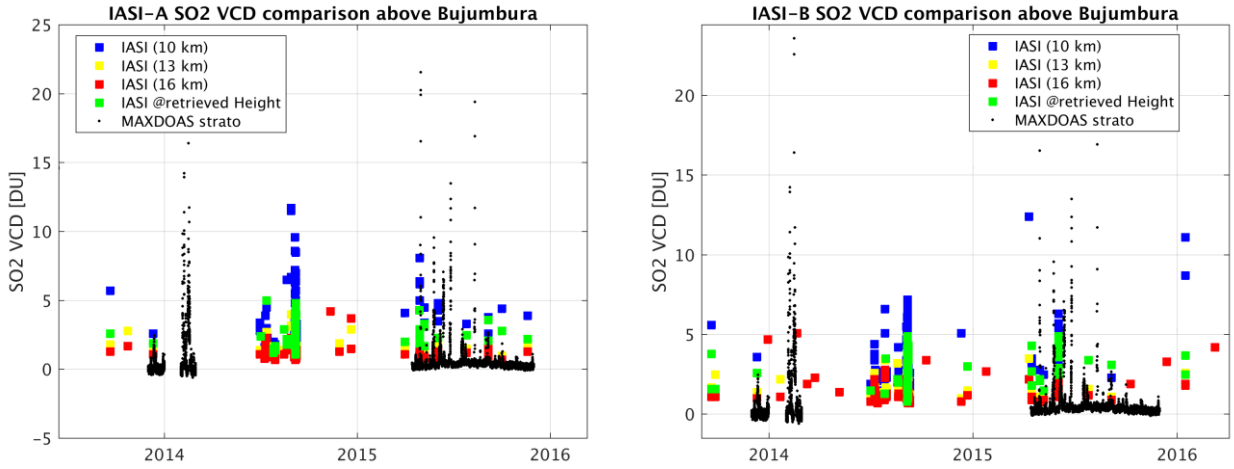

Figure 15. Bujumbura SO_2 VCD time-series of the 2013-2016 IASI-A (left) and IASI-B (right) overpasses (colored squares and the available retrieved ground-based data (black dots).

The ground-based data were analysed for the 2013-2015 period, and data are presented in Figure 15. Unfortunately, there are several interruptions due to problems with the UV channel of the instrument (for e.g. in 2014, the data stops on the 26th of April and only starts again in April 2015) and the measurements stop on August 2017. Several SO_2 peaks are seen both in the IASI overpasses and in the ground-based signal, but the direct comparison is difficult because many peaks are not on the same days, probably due to some tropospheric SO_2 contamination of the ground-based dataset, and on the few common days (10 Dec-2013, 30-Apr-2015, 02-Jun-2015, 05-Sep-2015 and 01-Oct-2015) the IASI pixels with ΔBt >1K are quite distant from the station (up to 300km), as shown in Figure 16.

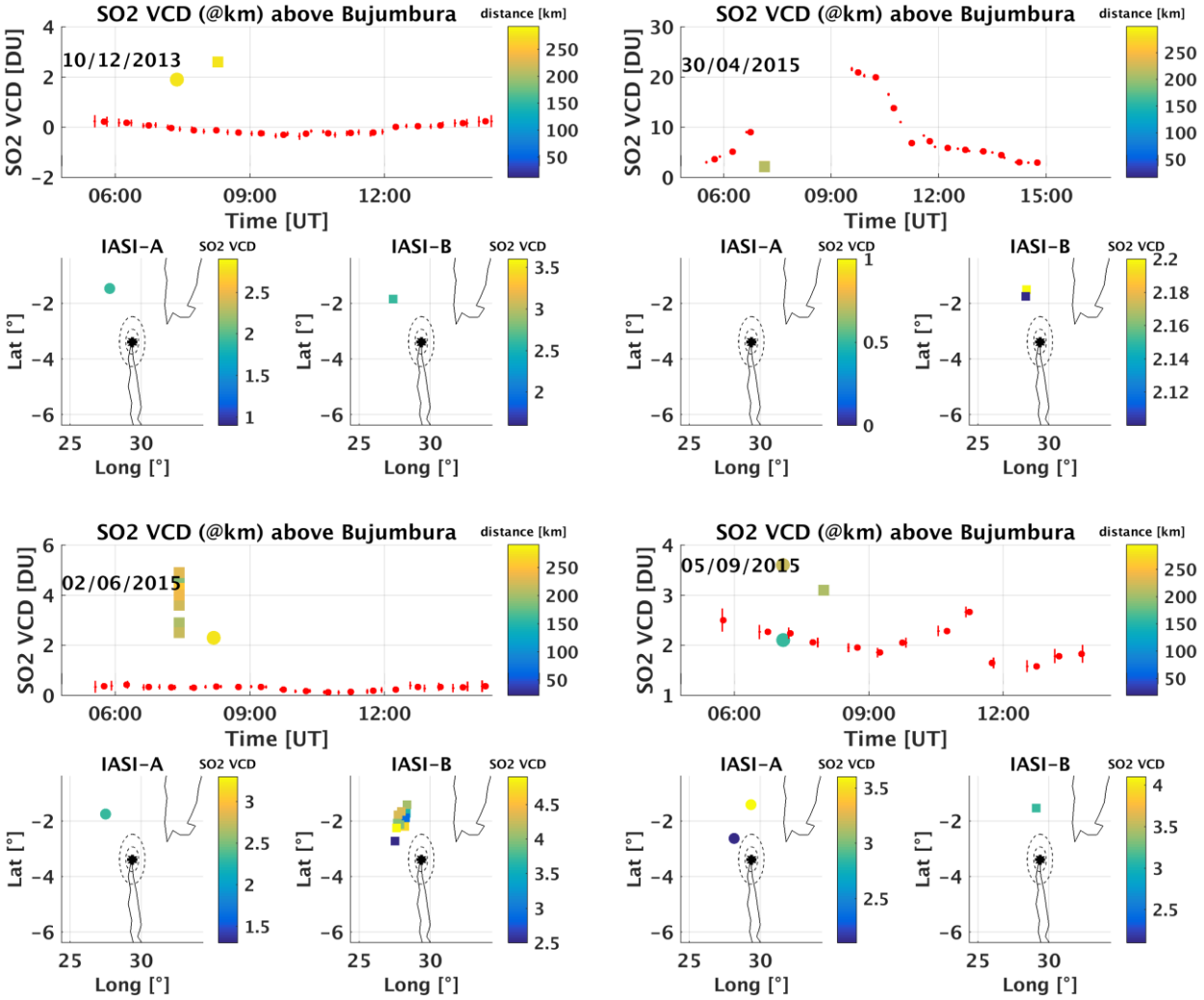

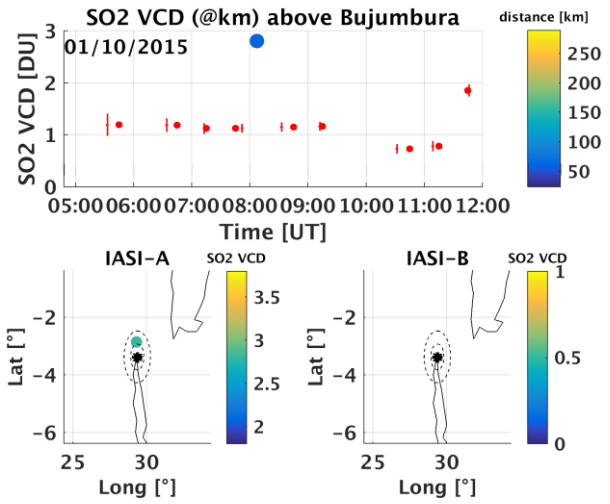

Figure 16. SO_2 VCD comparisons at Bujumbura for different eruptive days. The figure presents an upper panel, with the SO_2 VCD time-series from the zenith measurements (in red) and from IASI-A (circles) and IASI-B (squares) (SO_2 columns at the retrieved height, color-coded as a function of the station distance). The lower panels present the geographical distribution of the IASI-A (left) and IASI-B (right) SO_2 VCD around the station (circles at 50km and 100km are plotted in dotted lines).

Reunion

An illustration of the IASI-A overpass for Reunion is given in Figure 17 for the whole time-series (left) and for 23th of July 2019, when the Ubinas eruption plume passed close to the Reunion island in the right (https://volcano.si.edu/showreport.cfm?doi=GVP.WVAR20190724-354020).

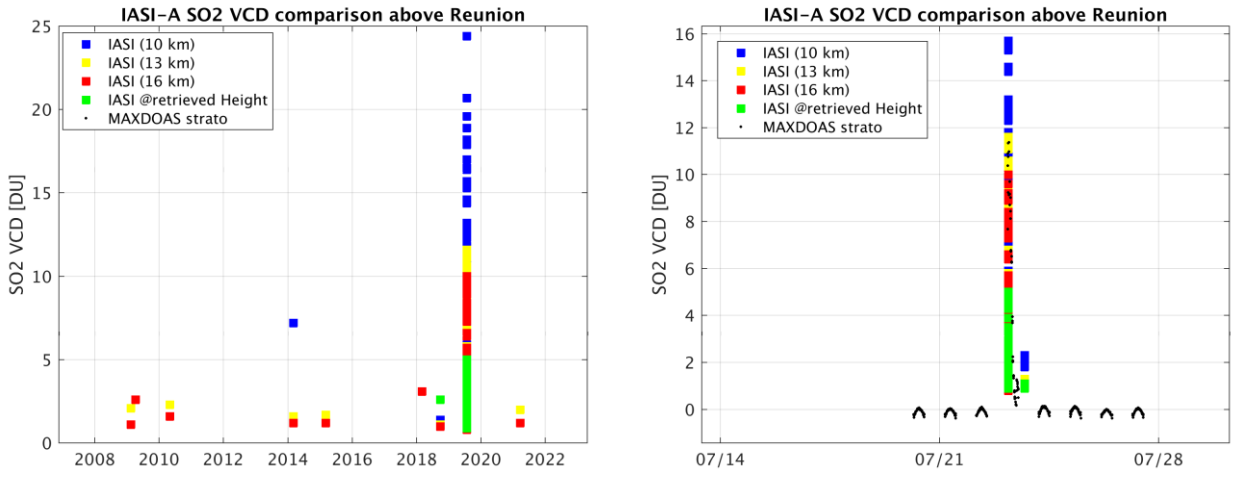

Figure 17. Reunion SO_2 VCD time-series of the IASI overpasses (colored squares) and the analyzed ground-based data (black dots). Left: the whole 2007-2021 time-series; Right: zoom on July 2019 for the Ubinas plume on the 23th.

BIRA-IASB measured with a MAXDOAS in LePort (on the coast) between April 2016 and January 2018, and then moved the instrument to the Maido site (at 2360m) and has been measuring there since June 2018. The data from the Maido site are thus compared to the SO_2 at the retrieved altitude for the IASI-A and IASI-B overpasses in Figure 18. It can be seen that on the 23/07/2019, during the day the

SO_2 from the ground-based decrease from about 10DU in the morning to about zero later in the day (from 9h UT). Similarly, the SO_2 values decrease from the IASI-A to the IASI-B overpass time (around half an hour later).

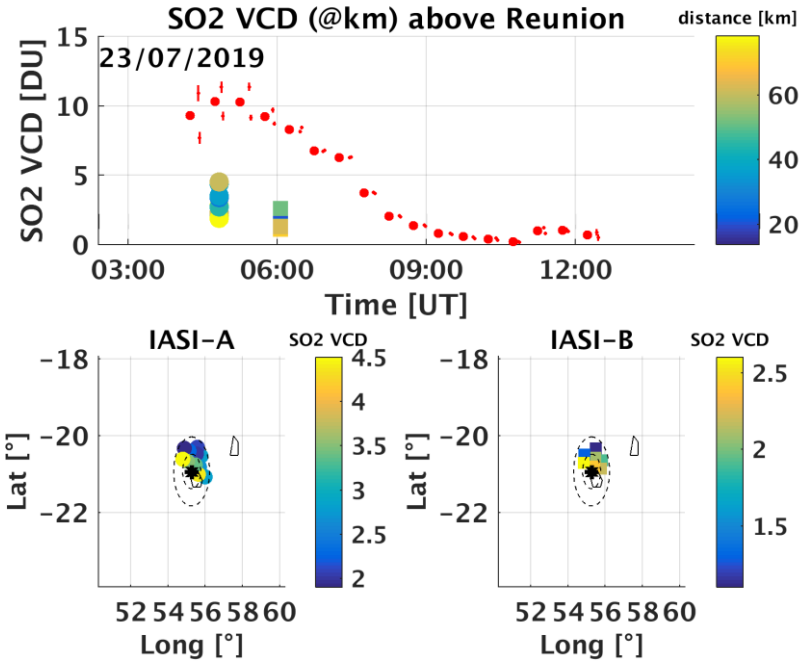

Figure 18. SO_2 VCD comparisons at Reunion focusing on the Ubinas eruption on 23/07/2019. The figure presents an upper panel, with the SO_2 VCD time-series from the zenith measurements (in red) and from IASI-A (circles) and IASI-B (squares) (SO_2 columns at the retrieved height, color-coded as a function of the station distance). The lower panels present the geographical distribution of the IASI-A (left) and IASI-B (right) SO_2 VCD around the station (circles at 50km and 100km are plotted in dotted lines).

Xianghe

Figure 19 present the time-series of the full IASI-A and IASI-B overpasses (upper row), and for June 2011 (first eruption after the installation of the MAXDOAS in 2010) during when the Nabro plume passed around the Xianghe station in the bottom left as well as in December 2020 in the bottom right.

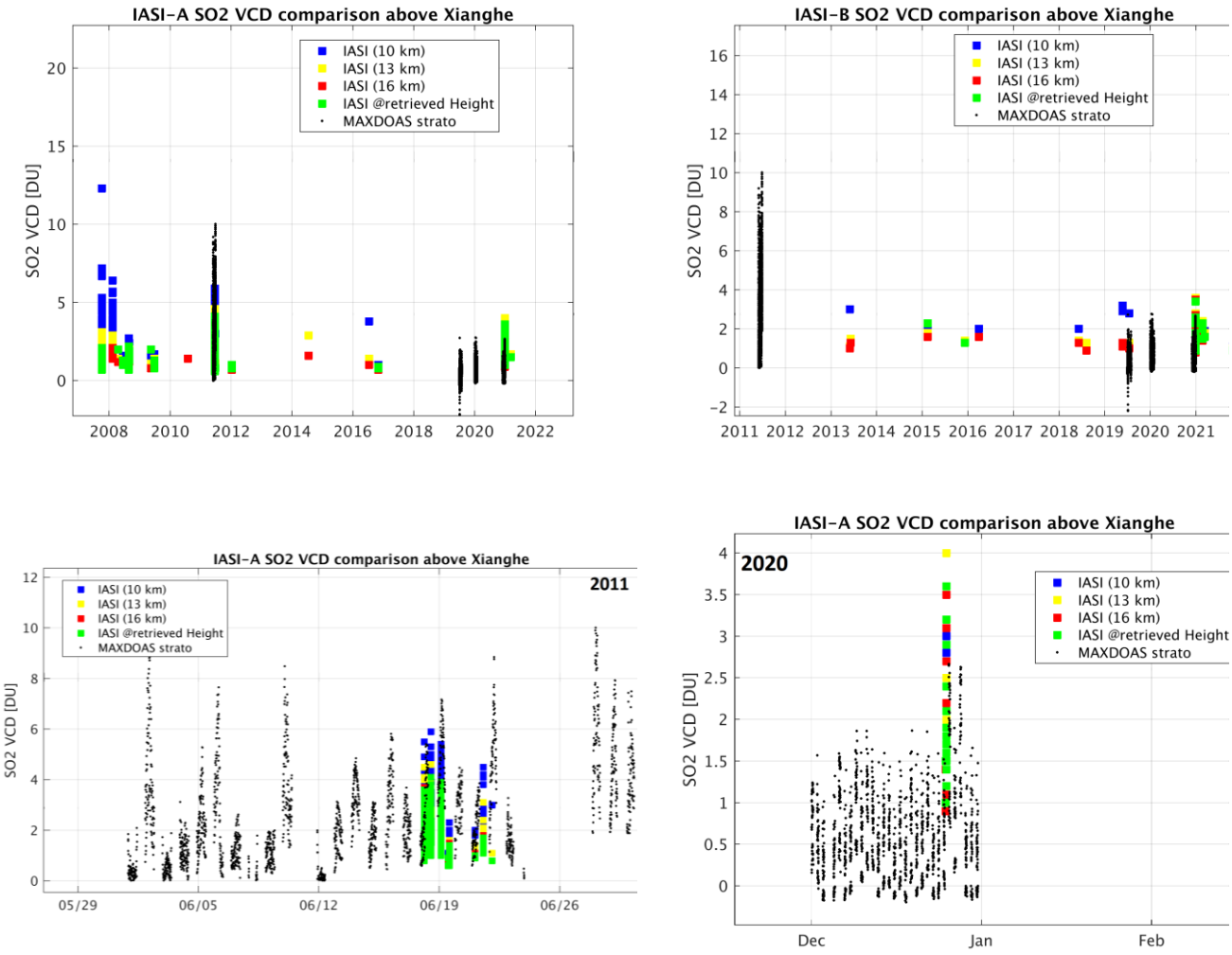

Figure 19. Xianghe SO_2 VCD time-series of the IASI-A and IASI-B overpasses (colored squares) and the analyzed ground-based data (black dots). Top row: the whole time-series; bottom: June 2011 Nabro eruption (left) and December 2020 (right).

As can be seen in Figure 19 for June 2011 and as discussed in past validation exercises [VR], the Xianghe station is more challenging because of the SO_2 pollution that is observed by the MAXDOAS instrument all year long (Wang et al., 2014), especially before 2018. This needs to be disentangled from the volcanic signal. To that end, an additional approach was tested, using also the direct sun and the MAXDOAS modes and comparing the results obtained in the different geometries. The direct sun total SO_2 VCD and the MAXDOAS tropospheric SO_2 columns from the profiling algorithm (Wang et al. 2014) are inter-compared (see Figure 20) and to the SO_2 VCD obtained using stratospheric VCD estimated from the zenith measurements using formula (2) as discussed before and performed for the other stations (see Figure 21 for the June 2011 period). Most of the time, the total SO_2 from the direct sun and the tropospheric SO_2 from the MAXDOAS profiling are very consistent, a sign that most of the SO_2 are in the lowest layers, sensed by both techniques. Some days, however, the direct sun signal is larger, sign of some additional (stratospheric) SO_2 content. The difference between the direct sun and the MAXDOAS data are compared in the lower plot of Figure 21. For days where both datasets agree well, we are confident of the retrieved stratospheric SO_2, and this can be compared to IASI SO_2 data, as shown in Figure 22. The IASI plume height for the Nabro eruption has been estimated from

IASI in Clarisse et al., 2014 and is of about 16km around the Xianghe station on the 19 June 2011 (Clarisse et al., 2014, their Figure 10). The SO_2 at the retrieved height is shown in Figure 22 with also the SO_2 values estimated for heights from 10 to 16km, and it compare well with the SO_2 at 16km height, as expected. The IASI-A SO_2 columns at the retrieved height are thus compared day by day in Figure 23 to the ground-based data. When data with $\Delta Bt>1K$ exist, only the pixels within a radius of 80km around Xianghe are presented (18 and 19 June 2011), otherwise the pixels within 300km are shown.

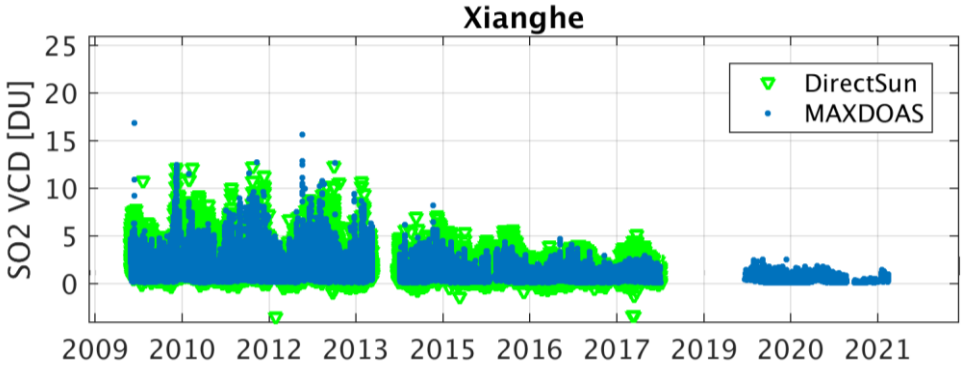

Figure 20. SO_2 VCD comparisons at Xianghe for total SO_2 from direct sun geometry (in green) and tropospheric SO_2 VCD from MAXDOAS (in blue).

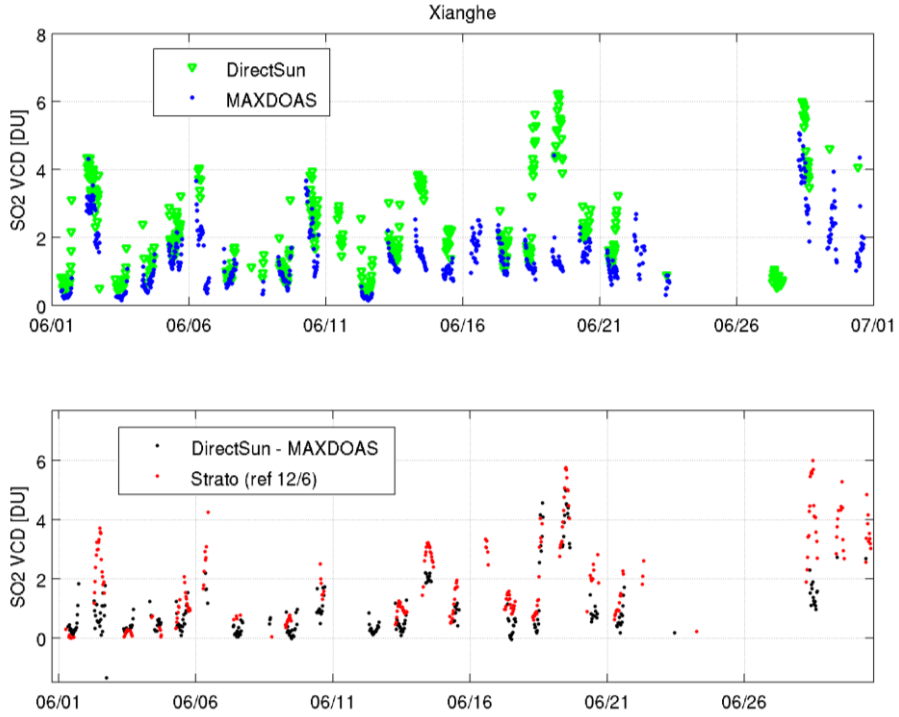

Figure 21. SO_2 VCD comparisons at Xianghe focusing on June 2011. The first panel shows total SO_2 from direct sun geometry (in green) and tropospheric SO_2 VCD from MAXDOAS (in blue). The second panel shows stratospheric SO_2, as retrieved from the total minus tropospheric VCD (in black) and as retrieved using a stratospheric AMF from zenith measurements (in red).

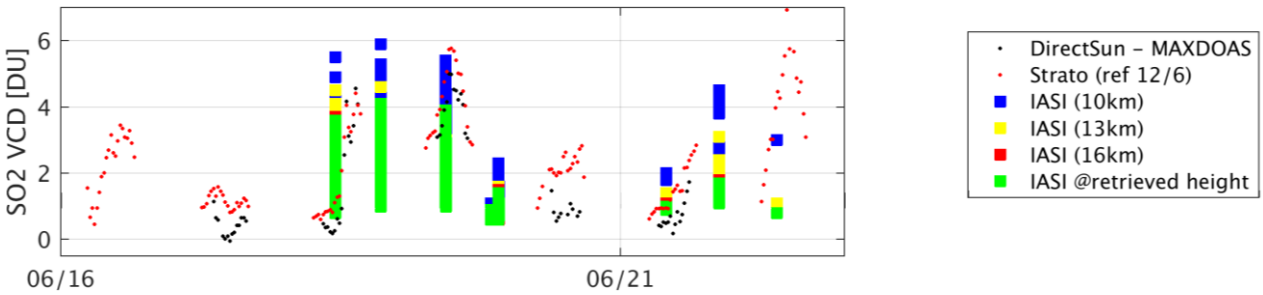

Figure 22. SO_2 VCD comparisons at Xianghe focusing on June 2011 around the Nabro plume overpass. IASI columns in a radius of 300km around the stations are reported for different heights and the stratospheric VCD are estimated from the total direct sun minus tropospheric MAXDOAS VCD (in black) and from zenith measurements with a fixed DOAS reference taken on 12/06/2011 at noon (in red).

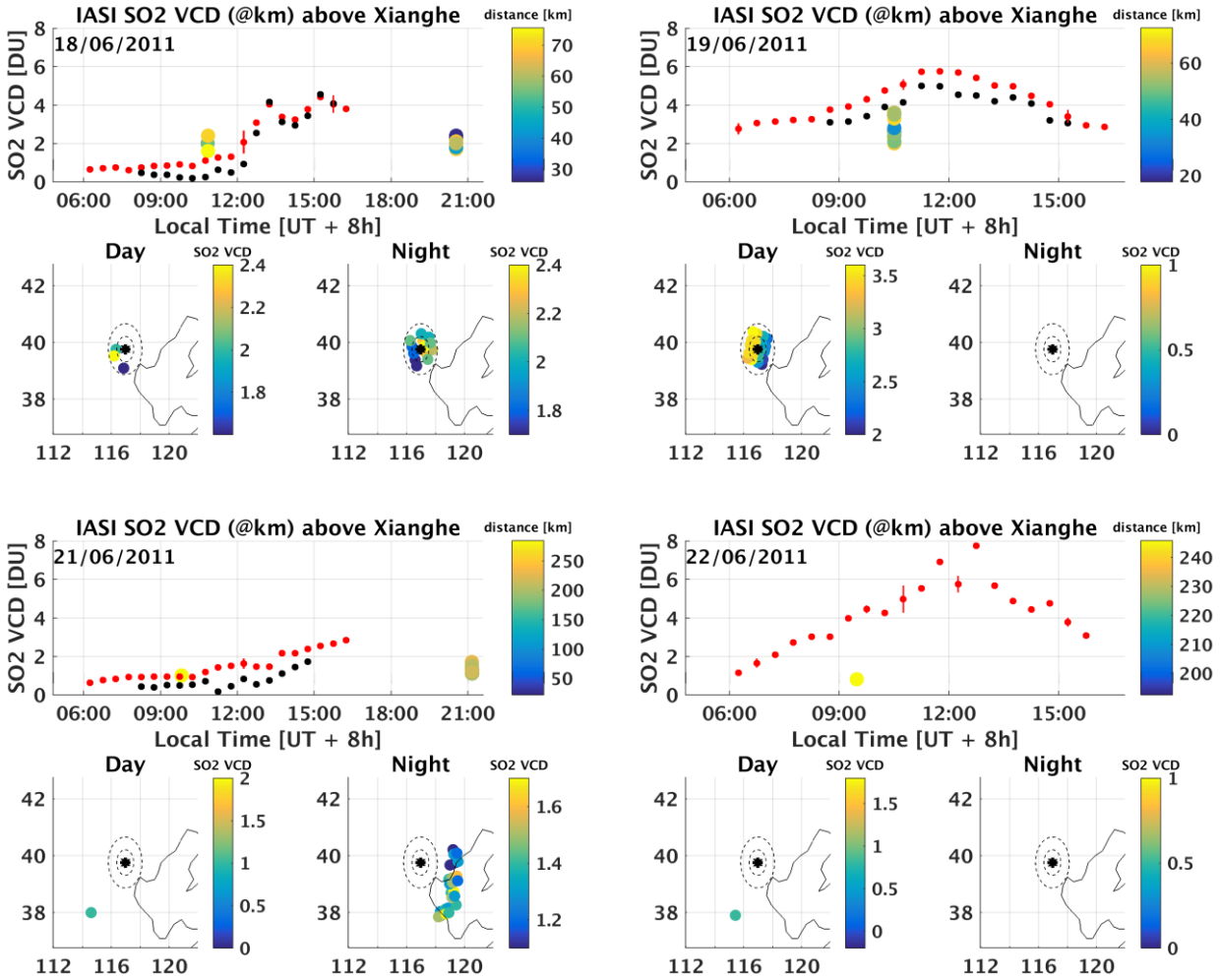

Figure 23. SO_2 VCD comparisons at Xianghe focusing on the 18 to 22 June 2011. Days are left to right, top to bottom. Each day present an upper panel, with the SO_2 VCD time-series reported from the total direct sun minus tropospheric MAXDOAS (in black), from the zenith measurements (in red) and from IASI-A (columns at the retrieved height, color-coded as a function of the station distance). The second panel presents the geographical distribution of the IASI SO_2 VCD around the Xianghe station (circles at 50km and 100km are plotted in dotted lines) for the day (left) and the night (right) overpasses.

From Figure 23, it can be seen that:

- the ground-based signal increases in the afternoon of 18/6/2011, from 2 to 4DU, comparable with the 2 to 2.5DU seen by IASI-A in the day and night overpasses;
- a stable to increasing signal on 19/6/2011 with 3 to 6 DU is seen by the ground-based, while 2 to 4 DU are seen by IASI during the morning overpass, with larger values for pixels west of the station;
- on the following days the SO_2 signal is reduced: no IASI-A signal on the 20 June and values are between 1 and 2 DU on 21 and 22 June, with a small number of pixels far away the station. From the ground, a signal between 1 and 2 DU is also seen on the 21 June, while on the 22 the signal is larger, but only data from the zenith measurements could be retrieved, so we trust less this day.

There are thus two good days to compare with, with two others have pixels too distant from the station. In this case, permitting also pixels with ΔBt between 0.4 and 1 (and not only >1K) increases the number of IASI pixels to compare with, however also increases the noise.

The volcanic signal in December 2020 is seen by both IASI-A and IASI-B, with some increase in the ground-based stratospheric VCD data (the direct sun mode was not working any more), but unfortunately, for both satellite instruments we only have a night overpass, as can be seen in Figure 24.

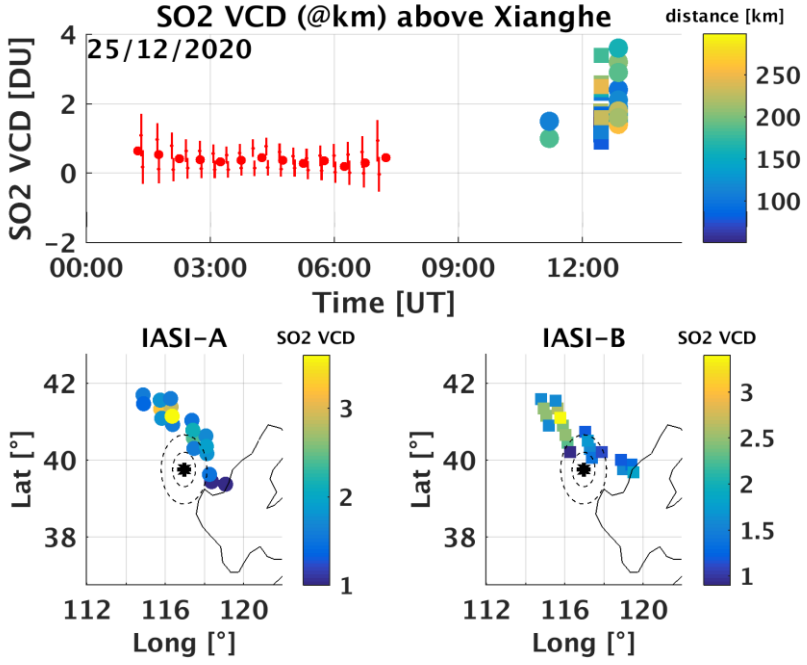

Figure 24. SO_2 VCD comparisons at Xianghe focusing on the 25 December 2020. In the upper panel, the SO_2 VCD time-series are reported from the zenith measurements (in red) and from IASI-A (dots) and IASI-B (squares) (SO_2 columns at the retrieved height, color-coded as a function of the station distance). The lower panels present the geographical distribution of the IASI-A (left) and IASI-B (right) SO_2 VCD around the Xianghe station (circles at 50km and 100km are plotted in dotted lines) for the day (left) and the night (right) overpasses.

3.2.1 Conclusions from the comparisons with the BIRA-IASB ground-based stations

Although the relatively small number of valid coincident cases (only 8 IASI-A and 5 IASI-B comparison days within pixels within 80km of the stations), qualitatively there seems to be a good agreement, with ground-based stations generally showing enhanced SO_2 signals just before/during/after the enhanced IASI SO_2 overpasses and the order of magnitude of the SO_2 signals are generally comparable. IASI-A and IASI-B usually display SO_2 temporal variations coherent with what seen from the ground.

To look at the results in a more quantitative way, we can average the ground based SO_2 data for half an hour around the IASI overpass time (±15min) and compare them to the mean SO_2 VCD loads from the selected IASI pixels (see Figure 25 for an illustration). We can do this exercise for the different IASI SO_2 VCD estimates, based on the fixed 7 to 25km heights and on the retrieved altitude. The resulting mean SO_2 VCD are summarized in Table 4 and Table 5 for IASI-A and IASI-B respectively. Please note that due to the ±15min temporal coincidence restriction, some of the cases presented above are not retained here (e.g., Bujumbura on 1/10/2015).

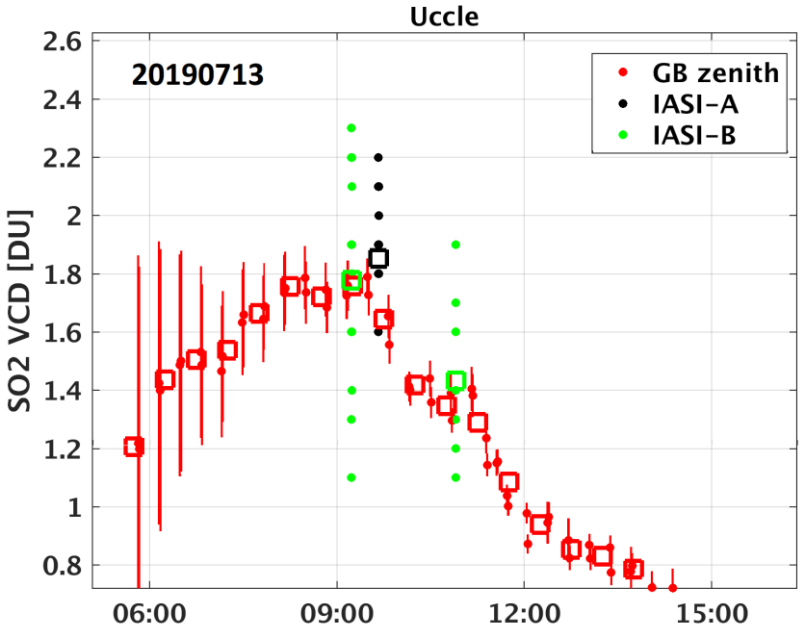

Figure 25. Illustration of the quantitative comparison method for Uccle on 13/07/2019, taking 30-minutes averages (squares) from the original ground-based and IASI datasets.

Table 4. Mean SO_2 VCD values for the ground-based and IASI-A different options, for the good condition cases (pixels from daily overpass within 80km of the station).

IASI-A				SO_2 VCD [DU]						
year	month	day	Station	GB	retrieved height	7km	10km	13km	16km	25km
2011	6	18	Xianghe	1,48	2,00	7,10	3,03	2,53	2,13	2,43
2011	6	19	Xianghe	5,43	2,99	8,52	4,24	3,10	2,96	3,43
2019	7	13	Uccle	1,66	1,85	4,26	1,92	1,90	1,62	1,78
2019	7	14	Uccle	1,09	1,78	3,33	2,20	1,84	1,61	1,68
2011	6	6	JFJ	1,88	1,50	n/a	1,70	1,40	1,20	1,40
2013	11	24	JFJ	0,59	0,80	1,78	0,83	0,83	0,82	0,70
2019	7	23	Reunion	10,28	2,95	20,62	11,19	5,57	4,87	6,47

Table 5. Mean SO_2 VCD values for the ground-based and IASI-B different options, for the good condition cases (pixels from daily overpass within 80km of the station).

IASI-B				SO_2 VCD [DU]						
year	month	day	Station	GB	retrieved height	7km	10km	13km	16km	25km
2019	7	9	Uccle	0,69	1,43	4,50	1,57	1,40	1,30	1,43
2019	7	13	Uccle	1,76	1,78	4,48	1,79	1,76	1,48	1,63
2019	7	13	Uccle	1,33	1,43	4,53	1,57	1,46	1,26	1,41
2019	7	14	Uccle	0,84	1,46	3,14	1,76	1,38	1,16	1,28
2019	7	14	Uccle	1,37	1,54	3,66	2,16	1,60	1,40	1,55
2013	11	24	JFJ	0,74	0,78	1,86	0,72	0,82	0,74	0,66
2019	7	23	Reunion	8,61	1,94	16,67	8,94	4,52	3,81	4,92

Generally, the results are very similar for IASI-A and IASI-B, with a good agreement of the ground-based data with the IASI SO_2 VCD at the retrieved altitude for moderate SO_2 content (cases with SO_2 VCD below 5 DU). Larger differences appear for the Reunion 23/7/2019 case and the Xianghe 19/6/2011 case, which have ground-based columns around 10 and 5 DU respectively, while IASI retrieve smaller SO_2 values when considering the retrieved altitude. The SO_2 estimate for 10km height appears closer to the ground-based values.

The summary result comparisons for all the cases together are presented in Figure 26 for the IASI SO_2 VCD at the retrieved altitude and for the 10km altitude assumption. Correlation coefficients are very good (about 0.82/0.63 for IASI-A and IASI-B and up to 0.97/0.99 for the 10km assumption) with linear regression slope close to one in the second case.

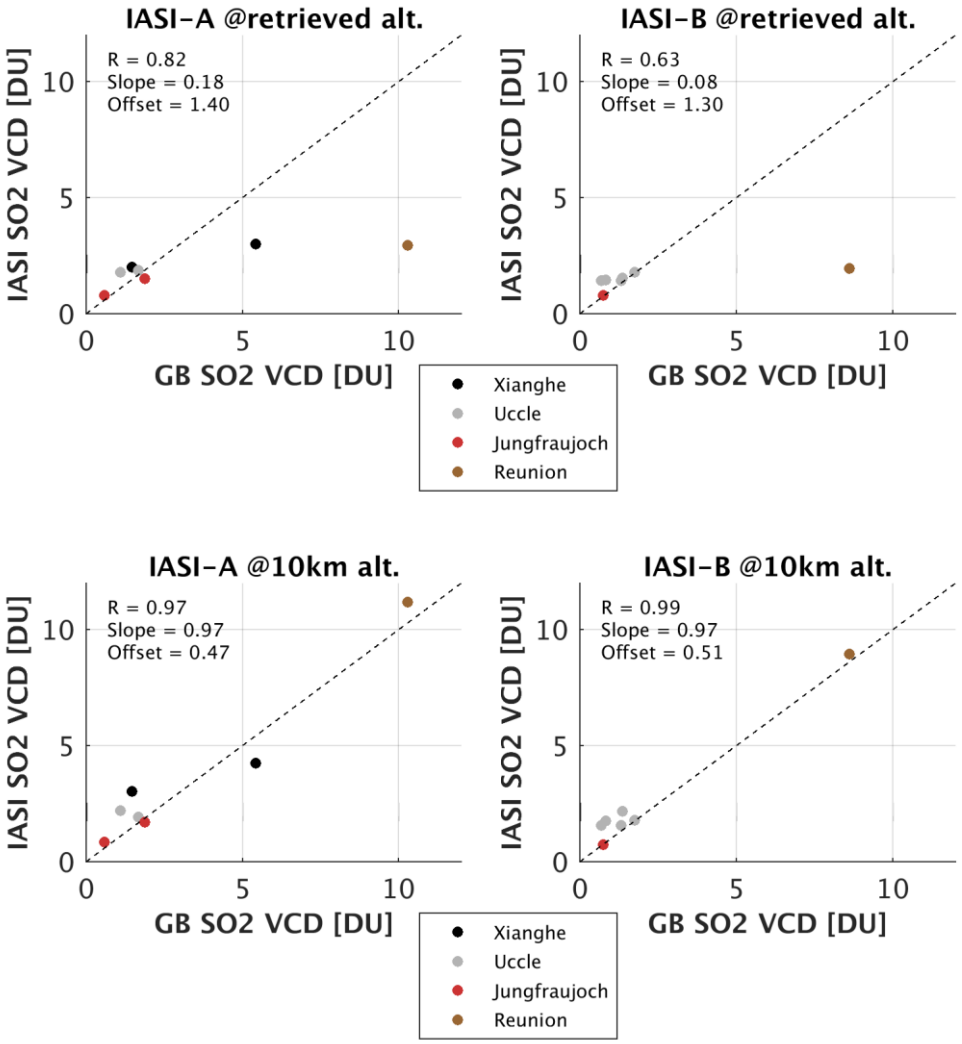

Figure 26. SO_2 VCD comparisons summary for the different IASI SO_2 estimates: SO_2 retrieved height (upper) and fixed 10km height (lower) for IASI-A (left) and IASI-B (right).

4. SULPHUR DIOXIDE ALTITUDE VALIDATION

Accurate determination of the location, height and loading of SO_2 plumes emitted by volcanic eruptions is essential for aviation safety. The SO_2 layer height is furthermore one of the most critical parameters that determine the impact on the climate. The height of volcanic ash columns are often estimated by local observers with mostly unknown accuracy. The plume height can also be determined using aircraft, ground-based radar or LIDAR but such observations are often not available and many volcanic eruptions in remote areas remain not observed. In addition, volcanic plumes containing SO_2 but not ash cannot be seen directly by either ground-based or space-born lidars.

SO_2 in the atmosphere has important impacts on chemistry and climate at both local and global levels. Natural sources account for ~30% of SO_2 emissions. Next to contributions from volcanic activity, these include emissions from marine phytoplankton and a small contribution from soil and vegetation decay. However, by far the largest contributions in global SO_2 production are from anthropogenic sources. These account for the remaining 70% of global emissions and primarily relate to fossil fuel burning, with smaller contributions from smelting and biomass burning.

4.1.1 S5P/TROPOMI SO_2 Layer Height

While satellite instruments, in principle, provide global products e.g. from SEVIRI (Second Generation Spin-stabilised Enhanced Visible and Infra-Red Imager) or AIRS (Atmospheric Infra-Red Sounder), they have no or little vertical resolution. Although retrievals of SO_2 plume height have been carried out using satellite UV backscatter measurements from e.g. OMI (Ozone Monitoring Instrument) or GOME2, until now such algorithms are up to now very time-consuming, since the spectral information content and its characterization require computationally demanding radiative transfer modelling. Due to the high spatial resolution of TROPOMI (Tropospheric Ozone Measurement Instrument) aboard S5P (Sentinel-5p) and consequent large amount of data, an SO_2 layer height algorithm has to be very fast. The Sentinel-5P Innovation project (S5p+I) has been initiated to develop novel scientific and operational applications, products and retrieval methods that exploit the potential of the Sentinel-5p mission's capabilities beyond its primary objective. The SO_2 Layer Height (SO_2LH) theme was dedicated to the generation of an SO_2 layer height product for Sentinel-5p taking into account data production timeliness requirements. In this report, we will compare the ESA S5P+I SO_2 Layer Height product, which is based on the algorithm of Efremenko et al., 2017, further improved by Hedelt et al., 2019, validated by Koukouli et al., 2022 and assimilated successfully into the CAMS forecasting system, as demonstrated by Inness et al., 2022.

The S5P SO_2 LH data are available upon request from the ESA S5P+I: SO2LH project Data Pool[2] where the final version of the SO_2 LH data, v4.0, is available. We should note here that this algorithm will be implemented during 2023 into the operational ESA MPC-ATM S5P dataset chain and will be part of the operational S5P SO_2 dataset from 2024 onwards. Due to restrictions of the algorithm, discussed in Hedelt et al., 2019 and Koukouli et al., 2022, a number of flags are applied to the dataset for quality assured results. The main one affecting this analysis is about the retrieved SO_2 load by the algorithm which is set to be > 20 D.U. As a result, shown in the section below, a number of the thinner SO_2 plumes observed by the IASI instruments which have no such restriction, are missing from the S5P SO_2 LH data.

[2] Data pool | Sentinel-5p Innovation (dlr.de)

4.1.2 Volcanic eruptions studied

For the requirements of this report, five major eruptions during the common timeline of S5P and IASI are studied. In detail:

- On **22 June 2019** at 04:00h local time, the **Raikoke** stratovolcano located on the Kuril Islands (Russia, 551 m summit elevation) erupted explosively (VEI ≥ 4) after being dormant since 1924. There were several strong distinct explosions, producing a dense ash and SO_2 plume that rose until 13 km altitude the first days and was entrained into the stratosphere (see Sennert, 2019). This was the strongest volcanic eruption since the Merapi eruption in 2011, producing a colossal SO_2 plume with an SO_2 loading of more than 900 DU on 22 June 2019, that was dispersed by strong winds over Russia and North America, and was detectable even two weeks after the volcanic eruption. MLS was able to perform SO_2 profile measurements and also CALIPSO was able to detect the ash plume during the first days after the eruption.

- The **Taal** Volcano in Batangas, Philippines erupted on the afternoon of **January 12th, 2020**, 43 years after its previous eruption in 1977. Stronger explosions began around 3 pm that spewed an ash column exceeding a kilometre high. By 7:30 pm, volcanic activities intensified as continuous eruptions generated a tall 10 to 15 kilometres steam-laden tephra column. On January 13, the activity on Taal's main crater had transitioned into a lava fountain.

- **Nishinoshima** lies about 600 miles (1,000 km) south of Tokyo, Japan, in the Ogasawara Arc. A young volcano, it has gone through several expansions in recent history. During a major eruption in 1973-1974, several new islands coalesced and expanded the size of the small island. In 2013, another vigorous eruption, which began offshore and continued until late 2015, eventually covered the island with lava flows and again enlarged the island. The volcano has been increasingly active through most of 2020, with **July 2020** seeing extreme activity, including a series of powerful vulcanian-type eruptions from July 30-August 1st, characterized by dense, ash-rich cloud of gas exploding from the volcanic crater and typically rising high above the peak.

- On the morning of **April 9th 2021**, **La Soufrière** volcano, on the Caribbean island of Saint Vincent, began erupting, spewing ash at least 25,000 feet in the air. The volcano continued to erupt over the next several days, with multiple violent explosions. Ash blanketed Saint Vincent and winds carried ash to Barbados, about 120 miles east. A violent eruption on April 12th generated pyroclastic flows, a high-density mix of hot lava blocks, pumice, ash, and volcanic gas that moves at very high speeds down volcanic slopes. La Soufrière last erupted in 1979.

- **Mt Etna,** in Sicily, is a continuous outgassing volcano and one of the tallest active volcanoes in Europe. Beginning in **February 2021**, Mount Etna began a series of explosive eruptions, which have had an impact on nearby villages and cities, with volcanic ash and rock falling as far away as Catania. As of 12 March 2021, the volcano has erupted 11 times in three weeks. The eruptions have consistently sent ash clouds over 10 km (33,000 ft) into the air, closing Sicilian airports.

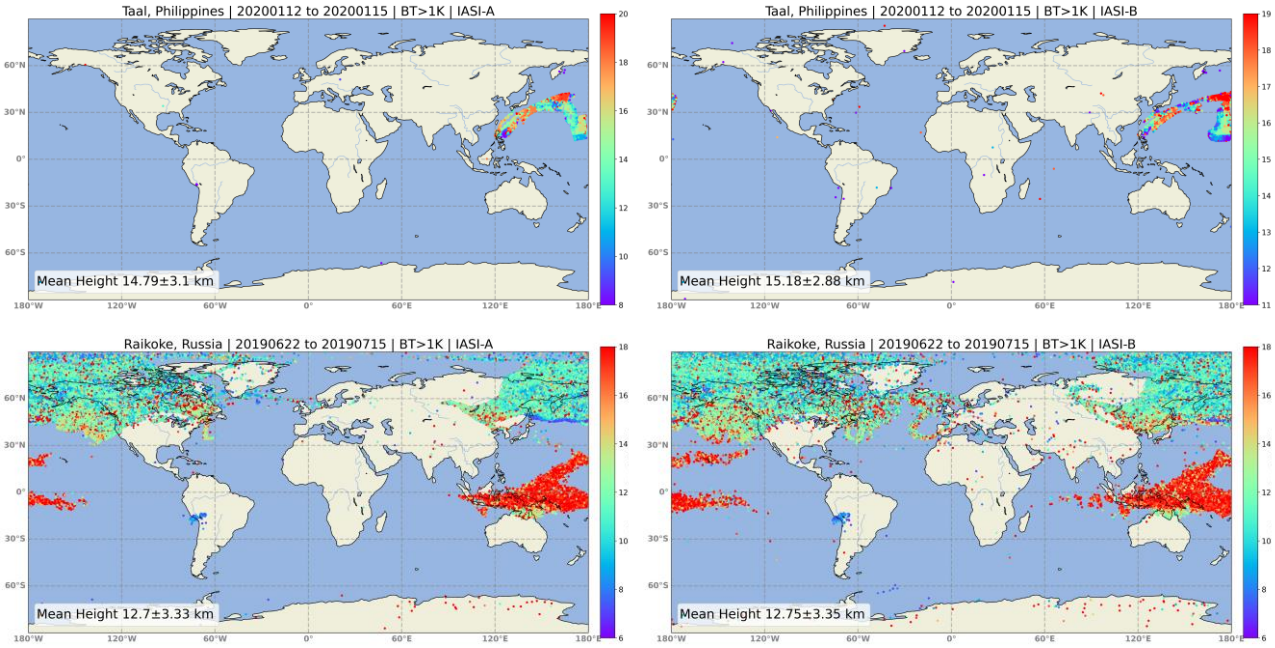

Figure 27. Examples of the IASI-A [left] and IASI-B [right] ΔBt > 1K SO_2 plume height during the Taal 2020 eruption [upper] and the Raikoke 2019 eruption [lower]. Note that during Raikoke, there was a synchronous volcanic eruption in Indonesia.

4.1.3 Comparisons with the S5P/TROPOMI SO_2 layer height

In Figure 28 and Figure 29 we present two example days of the Raikoke eruption for demonstrational purposes. In the former the second day of the eruption is shown, the 24th of June 2019, while in the latter, the fifth day, the 27th of June 2019. In the upper panels the S5P SO_2 layer heights are presented, while IASI-A and IASI-B follow. The left column contains IASI data with ΔBt > 0.4 K and the right ΔBt > 1K. Two main features are revealed by these pictorial investigations:

- The thickest, central, parts of the SO_2 plume appear to be missing from the IASI SO_2 plume heights shown in Figure 28. This part contains the highest SO_2 loads, within one day from the main eruption. Similarly, S5P is unable to sense the thinner filament-like plumes revealed by IASI due to the minimum SO_2 load constraint imposed by the algorithm, as discussed above.
- This issue is even more pronounced in Figure 29 where IASI reports on the spread of the volcanic plume over a wide geographical range, which is not picked up by S5P.

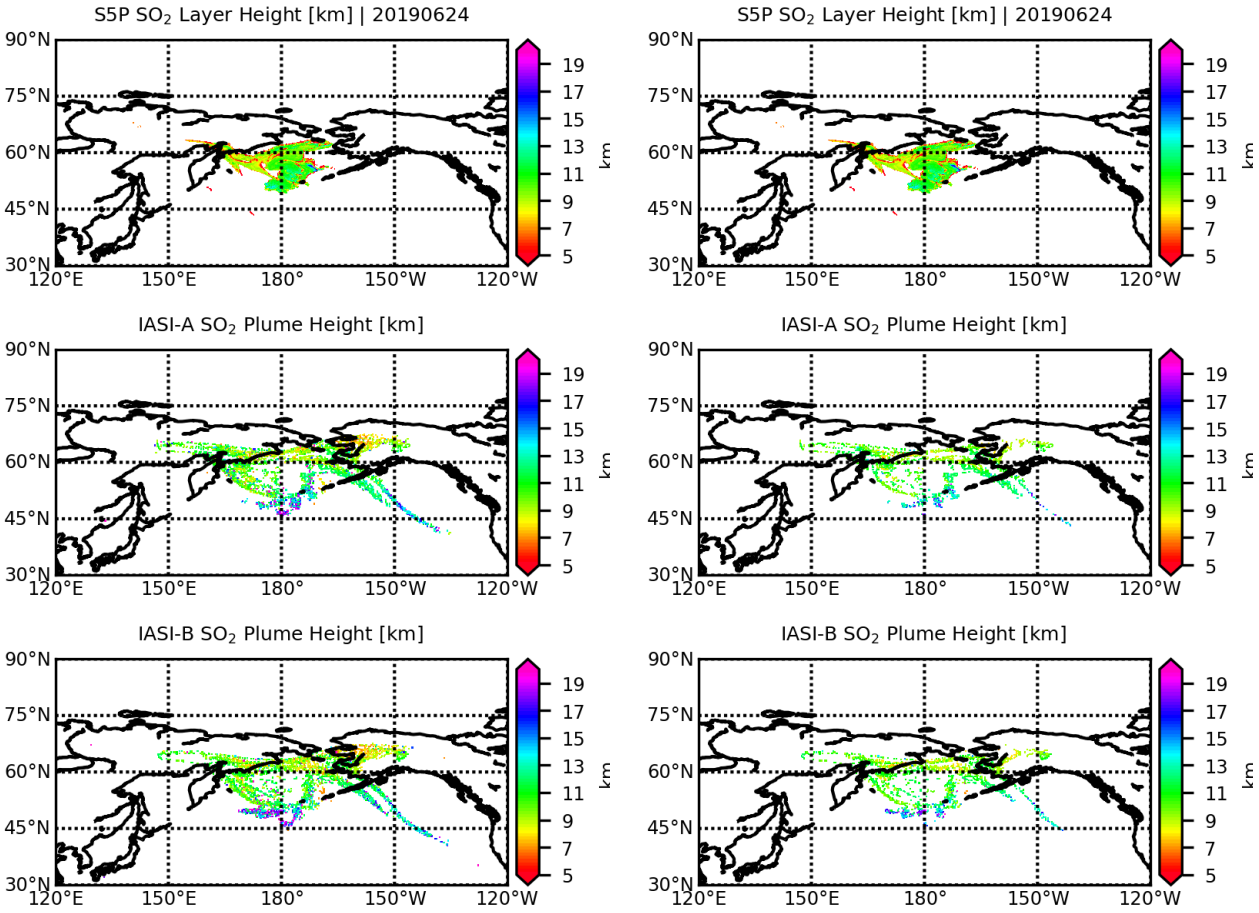

Figure 28. The second day of the Raikoke eruption, on the 24th of June 2019, is shown for the S5P SO_2 layer height [upper], the IASI-A SO_2 plume height [middle] and the IASI-B SO_2 plume height [lower] for IASI data with $\Delta Bt > 0.4$ K [left column] and $\Delta Bt > 1$K [right column.]

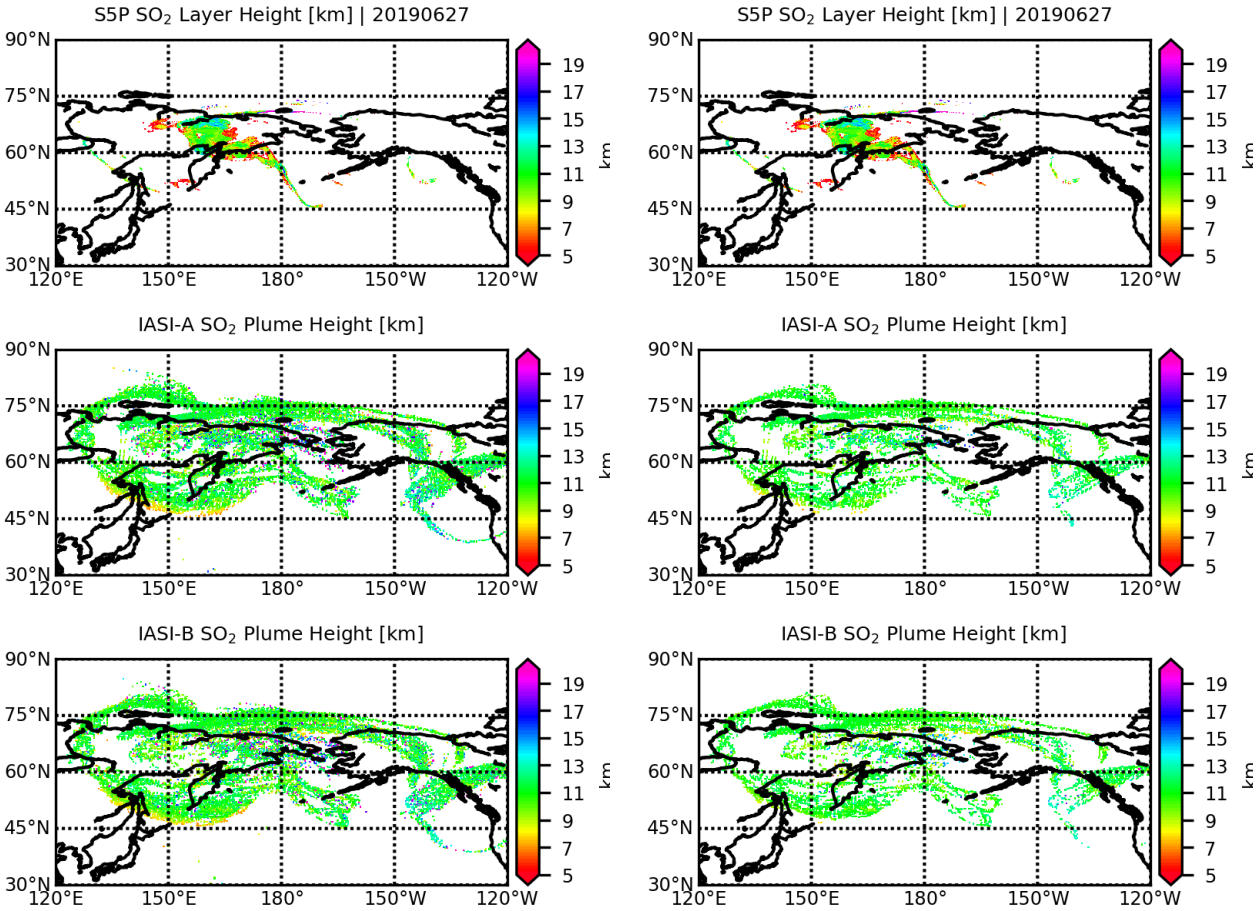

Figure 29. The fifth day of the Raikoke eruption, on the 27th of June 2019, is shown for the S5P SO_2 layer height [upper], the IASI-A SO_2 plume height [middle] and the IASI-B SO_2 plume height [lower] for IASI data with ΔBt > 0.4 K [left column] and ΔBt > 1K [right column.]

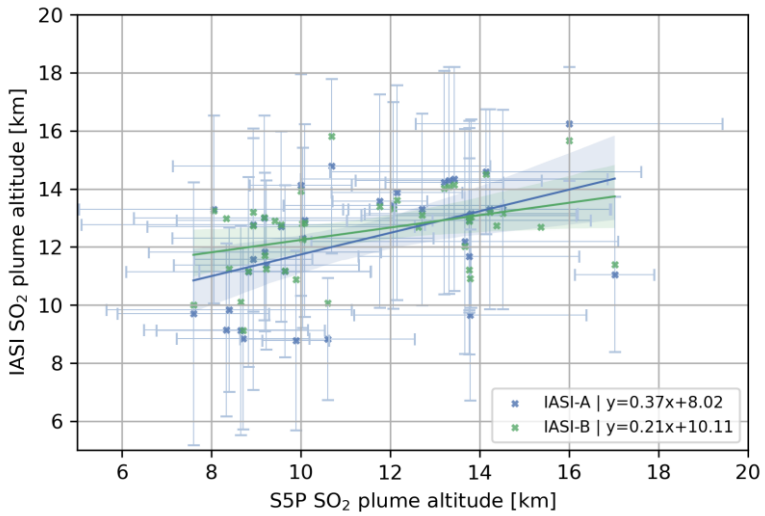

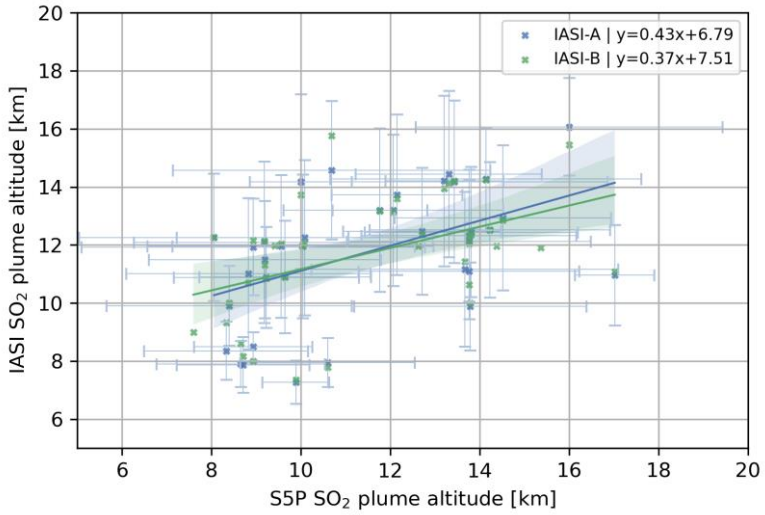

Figure 30. Scatter plot of the daily mean SO_2 heights sensed by S5P, IASI-A [blue] and IASI-B [green] for all eruptive periods enumerated in **Table 6**. Upper plot for IASI data with ΔBt > 0.4 K and lower plot for IASI data with ΔBt > 1.0 K.

In Figure 30, scatter plots of the daily mean SO_2 heights sensed by S5P compared separately to IASI-A and IASI-B are presented. The stricter flagging of the IASI data with ΔBt > 1.0 K improves both the slope and y-intercept of the comparisons, shown insert in the figures. In detail, for the comparison to IASI-A with ΔBt > 1.0 K, the S5P SO_2 heights range between 8.06 and 17.02km, while IASI-A range between 7.27 and 16.07km for the 37 collocation days with a correlation coefficient of 0.50. For the comparison to IASI-B with ΔBt > 1.0 K, the S5P SO_2 heights range between 7.6 and 17.02km, while IASI-B range between 7.36 and 15.76km for the 43 collocation days and a correlation coefficient of 0.47.

When comparing with IASI-A, the mean S5P SO_2 height is 11.5±2.4 km and IASI-A 11.8±2.1km, while for IASI-B the mean heights are 11.5± 2.5km and 11.7±2.0km, respectively. We overall report that **the IASI-A and IASI-B SO_2 heights reside within 2.5km from the S5P SO_2 height estimates**, well within the currently acceptable ranges for this product.

5. SUMMARY AND RECOMMENDATIONS

The dual aim of this validation report is to assert the capability of the EUMETSAT operational algorithm v6.6 to accurately retrieve IASI/MetopA and /MetopB total SO_2 columns and SO_2 plume heights on a global scale. For that end, Climate Data Recods (CDR) for IASI/MetopA between 01 Jan 2008 and 15 Oct 2021, and for IASI/MetopB between 20 Feb 2013 and 31 Dec 2021, were delivered by EUMETSAT to the validation teams.

In terms of the CDR netcdf files *per se*, we recommend that EUMETSAT considers in future releases to follow a more generic native-to-ncdf converter. Currently, differences in analysis were identified by the validation teams [not shown in this report] depending on which python module was employed in reading the CDR netcdf files. We further suggest the EUMETSAT considers releasing the IASI SO_2 CDR product in a harp-compliant netcdf format[3] in the future which would greatly increase the ease-of-use by the typical user.

In terms of assessing the suggested filtering on the SO_2 columns (section 2.2.1), we found that a number of pixels with high reported SO_2 columns are excluded when limiting the dataset to a $\Delta Bt > 1K$. Furthermore, we find the recommendation provided in the [PUM, section 5.2.2] that users *only look at the retrievals in the neighbourhood of so2_bt_difference > 1K pixels, and not use the pixels with a so2_bt_difference < 0.4K (not enough SO_2 to have a reliable retrieval). The size of the region around so2_bt_difference > 1K pixels is let to the user's estimate.* as non-viable for the typical user. We recommend that a volcanic flag is introduced in the dataset which will have a pre-defined region as "valid" which would still permit the expert user in making their own relevant calculations as they see fit for their work.

In terms of assessing the inter-sensor consistency (section 2.2.2) we report that both IASI-A ad IASI-B provide similar enough volcanic SO_2 retrieved columns which would enable the users to merge the two datasets and create a larger sample, always considering the temporal difference in their respective orbits.

In terms of comparisons against the S5P/TROPOMI volcanic SO_2 columns at an assumed plume height of 7km, section 3.1, we report that IASI-A and IASI-B nicely depict the major volcanic eruptions studied in this work, in terms of the location and spread of the plume on the day of, and following, the eruption. The overall levels of the IASI SO_2 retrieved columns are shown to be higher than those reported by S5P/TROPOMI both as SO_2 loads as well as SO_2 masses per day. Overall, we conclude that IASI-A and -B can be used in volcanic eruption monitoring and assessment.

In terms of comparisons against the BIRA MAX-DOAS ground-based observations, for the 8 IASI-A and 5 IASI-B temporally collocated days with pixels within 80km of the stations, a satisfactory agreement was found with correlation coefficients of about 0.82 for IASI-A and 0.63 for IASI-B for the retrieved SO_2 load and up to 0.97/0.99 for the SO_2 load with a 10km plume assumption.

In terms of the comparison of the IASI SO_2 plume height against the S5P/TROPOMI layer height, for five coincident eruptions, we report that when comparing with IASI-A, the mean S5P SO_2 height is 11.5±2.4 km and IASI-A 11.8±2.1km, while for IASI-B the mean heights are 11.5± 2.5km and 11.7±2.0km, respectively. We may hence conclude the IASI-A and IASI-B SO_2 heights reside within 2.5km from the S5P SO_2 height estimates, well within the currently acceptable ranges for this product.

We hence recommend the public release of this product.

[3] http://stcorp.github.io/harp/doc/html/ingestions/index.html

REFERENCES

Clarisse, L., Coheur, P.-F., Theys, N., Hurtmans, D., and Clerbaux, C.: The 2011 Nabro eruption, a SO_2 plume height analysis using IASI measurements, Atmos. Chem. Phys., 14, 3095-3111, doi:10.5194/acp-14-3095-2014, 2014.

Clarisse, L., Hurtmans, D., Clerbaux, C., Hadji-Lazaro, J., Ngadi, Y., and Coheur, P.-F.: Retrieval of sulphur dioxide from the infrared atmospheric sounding interferometer (IASI), Atmos. Meas. Tech., 5, 581-594, doi:10.5194/amt-5-581-2012, 2012.

Clemer, K., Van Roozendael, M., Fayt, C., Hendrick, F., Hermans, C., Pinardi, G., Spurr, R., Wang, P., and De Maziere, M.: Multiple wavelength retrieval of tropospheric aerosol optical properties from MAXDOAS measurements in Beijing, Atmos. Meas. Tech., 3, 863-878, 2010.

Dimitropoulou, E., Hendrick, F., Friedrich, M. M., Tack, F., Pinardi, G., Merlaud, A., Fayt, C., Hermans, C., Fierens, F., and Van Roozendael, M.: Horizontal distribution of tropospheric NO_2 and aerosols derived by dual-scan multi-wavelength multi-axis differential optical absorption spectroscopy (MAX-DOAS) measurements in Uccle, Belgium, Atmos. Meas. Tech., 15, 4503–4529, https://doi.org/10.5194/amt-15-4503-2022, 2022.

Dimitropoulou, E., Hendrick, F., Pinardi, G., Friedrich, M. M., Merlaud, A., Tack, F., De Longueville, H., Fayt, C., Hermans, C., Laffineur, Q., Fierens, F., and Van Roozendael, M.: Validation of TROPOMI tropospheric NO_2 columns using dual-scan multi-axis differential optical absorption spectroscopy (MAX-DOAS) measurements in Uccle, Brussels, Atmos. Meas. Tech., 13, 5165–5191, https://doi.org/10.5194/amt-13-5165-2020, 2020.

Efremenko, D.; Loyola, D.; Hedelt, P. and Spurr, R. (2017): Volcanic SO_2 plume height retrieval from UV sensors using a full-physics inverse learning machine algorithm. *International Journal of Remote Sensing*, Vol. 38 (50), pp. 1-27. Taylor & Francis, https://doi.org/10.1080/01431161.2017.1348644, ISSN 0143-1161.

Gielen, C., Hendrick, F., Pinardi, G., De Smedt, I., Fayt, C., Hermans, C., Stavrakou, T., Bauwens, M., Muller, J.-F., Ndenzako, E., Nzohabonayo, P., Akimana, R., Niyonzima, S., Van Roozendael, M., and De Maziere, M.: Characterisation of Central-African aerosol and trace-gas emissions based on MAX-DOAS measurements and model simulations over Bujumbura, Burundi, Atmos. Chem. Phys. Discuss., doi:10.5194/acp-2016-1104, in review, 2017.

Gielen, C., Van Roozendael, M., Hendrick, F., Pinardi, G., Vlemmix, T., De Bock, V., De Backer, H., Fayt, C., Hermans, C., Gillotay, D., and Wang, P.: A simple and versatile cloud-screening method for MAX-DOAS retrievals, Atmos. Meas. Tech., 7, 3509-3527, doi:10.5194/amt-7-3509-2014, 2014.

Hedelt, P., Efremenko, D. S., Loyola, D. G., Spurr, R., and Clarisse, L.: Sulfur dioxide layer height retrieval from Sentinel-5 Precursor/TROPOMI using FP_ILM, *Atmos. Meas. Tech.*, 12, 5503–5517, https://doi.org/10.5194/amt-12-5503-2019, 2019

Hendrick, F., Mahieu, E., Bodeker, G. E., Boersma, K. F., Chipperfield, M. P., De Mazière, M., De Smedt, I., Demoulin, P., Fayt, C., Hermans, C., Kreher, K., Lejeune, B., Pinardi, G., Servais, C., Stübi, R., van der A, R., Vernier, J.-P. and Van Roozendael, M.: Analysis of stratospheric NO_2 trends above Jungfraujoch using ground-based UV-visible, FTIR, and satellite nadir observations, Atmos. Chem. Phys., 12(18), 8851–8864, doi:10.5194/acp-12-8851-2012, 2012.

Hendrick, F., Muller, J.-F., Clamer, K., Wang, P., De Maziere, M., Fayt, C., Gielen, C., Hermans, C., Ma, J. Z., Pinardi, G., Stavrakou, T., Vlemmix, T., and Van Roozendael, M.: Four years of ground-based MAX-DOAS observations of HONO and NO2 in the Beijing area, Atmos. Chem. Phys., 14, 765-781, doi:10.5194/acp-14-765-2014, 2014.

Hendrick, F., Van Roozendael, M., Chipperfield, M. P., Dorf, M., Goutail, F., Yang, X., Fayt, C., Hermans, C., Pfeilsticker, K., Pommereau, J.-P., Pyle, J. A., Theys, N., and De Maziere, M.: Retrieval of stratospheric

and tropospheric BrO profiles and columns using ground-based zenith-sky DOAS observations at Harestua, 60° N, Atmos. Chem. Phys., 7, 4869-4885, doi:10.5194/acp-7-4869-2007, 2007.

Honninger, G., von Friedeburg, C. and Platt, U.: Multi axis differential optical absorption spectroscopy (MAX-DOAS), Atmos. Chem. Phys., 4, 231–254 [online] Available from: www.atmos-chem-phys.org/acp/4/231/, 2004.

Inness, A., Ades, M., Balis, D., Efremenko, D., Flemming, J., Hedelt, P., Koukouli, M.-E., Loyola, D., and Ribas, R.: Evaluating the assimilation of S5P/TROPOMI near real-time SO_2 columns and layer height data into the CAMS integrated forecasting system (CY47R1), based on a case study of the 2019 Raikoke eruption, Geosci. Model Dev., 15, 971–994, https://doi.org/10.5194/gmd-15-971-2022, 2022.

Koukouli, M.-E., Michailidis, K., Hedelt, P., Taylor, I. A., Inness, A., Clarisse, L., Balis, D., Efremenko, D., Loyola, D., Grainger, R. G., and Retscher, C.: Volcanic SO_2 layer height by TROPOMI/S5P: evaluation against IASI/MetOp and CALIOP/CALIPSO observations, Atmos. Chem. Phys., 22, 5665–5683, https://doi.org/10.5194/acp-22-5665-2022, 2022.

Moxnes, E. D., N. I. Kristiansen, A. Stohl, L. Clarisse, A. Durant, K. Weber, and A. Vogel (2014), Separation of ash and sulfur dioxide during the 2011 Grímsvötn eruption, J. Geophys. Res. Atmos., 119, doi:10.1002/2013JD021129.

Prata, F., Woodhouse, M., Huppert, H. E., Prata, A., Thordarson, T., and Carn, S.: Atmospheric processes affecting the separation of volcanic ash and SO2 in volcanic eruptions: inferences from the May 2011 Grimsvotn eruption, Atmos. Chem. Phys., 17, 10709-10732, https://doi.org/10.5194/acp-17-10709-2017, 2017.

Sennert, S. K., ed.: Report on Raikoke (Russia), Weekly Volcanic Activity Report, 19 June-25 June 2019, Global Volcanism Program, Smithsonian Institution and US Geological Survey, 2019. https://volcano.si.edu/showreport.cfm?doi=GVP.WVAR20190619-290250

Theys, N., Isabelle De Smedt, Christophe Lerot, Huan Yu and Michel Van Roozendael S5P/TROPOMI SO2 ATBD, , S5P-BIRA-L2-400E-ATBD, CI-400E-ATBD, issue: 2.4.1, date: 22.06.2022, https://sentinels.copernicus.eu/documents/247904/2476257/Sentinel-5P-ATBD-SO2-TROPOMI, last accessed: 03.04.2023

Valks, P., L. Chan, P. Hedelt, S. Slijkhuis and R. Lutz, ALGORITHM THEORETICAL BASIS DOCUMENT GOME-2 Total Column Products of Ozone, NO2, BrO, HCHO, SO2, H2O, OClO and Cloud Properties GDP 4.8 for GOME-2 on MetOp-A and -B GDP 4.9 for GOME-2 on MetOp-C, SAF/AC/DLR/ATBD/01, issue: 3/B , date: 11.11.2019, https://acsaf.org/docs/atbd/Algorithm_Theoretical_Basis_Document_NTO_OTO_Nov_2019.pdf, last accessed: 03.04.2023.

Valks, P., Pinardi, G., Richter, A., Lambert, J.-C., Hao, N., Loyola, D., Van Roozendael, M., and Emmadi, S.: Operational total and tropospheric NO2 column retrieval for GOME-2, Atmos. Meas. Tech., 4, 1491–1514, https://doi.org/10.5194/amt-4-1491-2011, 2011.

Wang, T., Hendrick, F., Wang, P., Tang, G., Clémer, K., Yu, H., Fayt, C., Hermans, C., Gielen, C., Müller, J.-F., Pinardi, G., Theys, N., Brenot, H. and Van Roozendael, M.: Evaluation of tropospheric SO2 retrieved from MAX-DOAS measurements in Xianghe, China, Atmos. Chem. Phys., 14(20), 11149–11164, doi:10.5194/acp-14-11149-2014, 2014.

APPENDIX

Table 6. Daily mean SO_2 height [km] for all eruptive days shown in Figure 30, bottom panel.

Eruptive volcano	Date	S5P SO_2 height [km]	IASI-A SO_2 height [km]	IASI-B SO_2 height [km]
	20200710	8.66±1.88	7.9±0.8	8.61±3.53
	20200711	8.71±1.48	7.87±0.96	8.17±2.03
	20200712	7.6±1.69	n/a	9.0±0.0
	20200713	8.33±1.83	8.35±1.0	9.33±0.47
	20200714	10.6±1.95	7.95±0.85	7.79±0.76
	20200715	13.79±2.6	9.88±1.52	10.0±1.41
	20200716	8.4±2.74	9.9±1.37	10.0±3.21
Nishinoshima	20200717	8.94±1.32	8.5±0.5	8.0±0.0
	20210410	14.14±3.48	14.27±1.77	14.24±1.76
LaSoufriere	20210411	16.0±3.43	16.07±1.68	15.45±1.78
Taal	20200113	10.69±3.55	14.57±2.39	15.76±2.16
	20190623	8.83±2.73	11.01±2.61	10.7±2.37
	20190624	9.65±1.92	10.9±1.94	10.89±2.27
	20190625	9.23±2.07	10.88±1.74	10.84±1.72
	20190626	9.2±2.6	11.5±2.02	11.31±1.77
	20190627	10.05±2.92	11.95±2.47	11.96±2.54
	20190628	9.56±2.99	11.95±2.46	12.04±2.59
	20190629	10.09±2.86	12.25±2.67	12.08±2.61
	20190630	9.18±2.91	12.09±2.78	12.14±2.84
	20190701	8.06±3.01	12.26±2.19	12.27±2.25
	20190702	8.94±3.84	11.93±1.67	12.16±2.03
	20190703	9.42±3.38	n/a	11.97±1.95
	20190704	10.03±3.4	n/a	11.98±2.08
	20190705	12.63±3.92	n/a	11.95±2.02
	20190706	14.38±5.14	n/a	11.95±2.01
	20190707	15.37±4.9	n/a	11.9±2.07
	20190708	13.76±2.73	12.12±2.12	12.05±2.12
	20190709	13.76±2.4	12.32±2.27	12.31±2.31
	20190710	13.81±2.38	12.44±2.24	12.35±2.28
	20190711	12.71±1.76	12.47±2.19	12.35±2.27
	20190712	14.23±2.69	12.52±2.33	12.52±2.42
	20190713	14.52±2.42	12.94±2.5	12.85±2.53
	20190714	12.07±2.46	13.19±2.61	13.14±2.6
	20190715	11.77±1.06	13.2±2.81	13.17±2.84
Raikoke	20190716	12.15±1.46	13.73±2.77	13.6±2.91

	20190717	10.0±1.14	14.18±3.0	13.72±2.94
	20190718	13.21±1.32	14.2±2.94	13.95±2.93
	20190719	13.31±2.08	14.44±2.87	14.12±2.92
	20190720	13.43±3.43	14.18±2.8	14.2±2.84
	20210221	13.76±2.47	11.1±1.66	10.63±1.87
	20210223	17.02±0.89	10.96±1.73	11.08±1.91
	20210304	13.67±3.43	11.16±2.66	11.43±2.72
Mt Etna	20210401	9.89±0.75	7.27±0.75	7.36±0.72